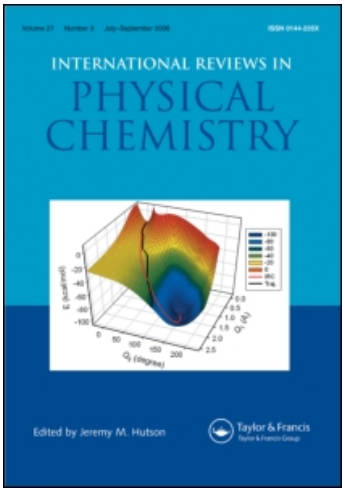

International Reviews in Physical Chemistry
Publication details, including instructions for authors and subscription information:
http://www.informaworld.com/smpp/title~content=t713724383

The observation of quantum bottleneck states

Rex T. Skodje[ab]; Xueming Yang[ab]
[a] Department of Chemistry and Biochemistry, University of Colorado, Boulder, CO 80309, USA and Institute of Atomic and Molecular Sciences, Academia Sinica, Taiwan [b] State Key Laboratory of Molecular Reaction Dynamics, Dalian Institute of Chemical Physics, CAS, Dalian, Liaoning 116023, P. R. China

To cite this Article Skodje, Rex T. and Yang, Xueming(2004) 'The observation of quantum bottleneck states', International Reviews in Physical Chemistry, 23: 2, 253 — 287
To link to this Article: DOI: 10.1080/01442350412331284616
URL: http://dx.doi.org/10.1080/01442350412331284616

INT. REVIEWS IN PHYSICAL CHEMISTRY, 2004
VOL. 23, NO. 2, 253–287

Taylor & Francis
Taylor & Francis Group

The observation of quantum bottleneck states

REX T. SKODJE*
Department of Chemistry and Biochemistry, University of Colorado, Boulder, CO 80309, USA and Institute of Atomic and Molecular Sciences, Academia Sinica, PO Box 23-166 Taipei, Taiwan

and XUEMING YANG
State Key Laboratory of Molecular Reaction Dynamics, Dalian Institute of Chemical Physics, CAS, Dalian, Liaoning 116023, P. R. China

The concept of quantum bottleneck states near reaction barriers is essential to the elucidation of chemical reaction rates and reaction dynamics. Recent studies of the dynamics of simple gas-phase chemical reactions have revealed that the transition state controls the detailed observable characteristics of a reaction to a far greater degree than was generally imagined. However, observation of such quantum bottleneck states is extremely difficult. In this article, we provide a review of the current status of observing these quantum bottleneck states in both bimolecular and unimolecular reactions, providing an updated picture of the concept of quantum bottleneck states in chemical reactions.

Contents

PAGE

1. Introduction 254

2. The theory of barrier passage 256
2.1. The quantum dynamics of one-dimensional barriers 257
2.2. Multidimensional bimolecular reactions 259

3. Strategies for observing quantum bottleneck states in reactive collisions 264
3.1. Forward scattering peaks: manifestations of time-delay 264
3.2. Energy oscillations in state-to-state differential cross-sections 271

4. Observing quantum bottleneck states in unimolecular reactions 276

5. Conclusions 285

Acknowledgements 285

References 286

* E-mail: skodje@spot.colorado.edu

International Reviews in Physical Chemistry ISSN 0144–235X print/ISSN 1366–591X online © 2004 Taylor & Francis Ltd
http://www.tandf.co.uk/journals
DOI: 10.1080/01442350412331284616

1. Introduction

Much of our understanding of the dynamics of chemical reactions is based on the concept of the transition state. For reactions occurring under thermally averaged conditions, transition state theory (TST) provides a fairly accurate predictive tool to compute the reaction rate constant [1]. The activation energy, pre-exponential factor and tunnelling coefficient of a reaction can usually be well modelled based on the local characteristics of the potential energy surface near the transition state. Our focus here, however, is on the utility of the transition state concept to interpret results obtained at a more detailed level, such as provided by molecular beam experiments, transition state spectroscopy, or laser photodissociation of jet-cooled molecules. While the dynamics of barrier crossing is obviously central to the process of chemical reaction, it remains unclear precisely how the properties of the transition state will imprint themselves upon the microscopic observables such as the differential cross-section (DCS). Recently, however, experiments and theory have begun to reveal certain aspects of the connection between laboratory observation and the quantum dynamics near the transition state. In this review, we discuss the recent progress that has been made in observing and interpreting the quantum structure of the transition state. A central theme of this work is a discussion of how the discrete spectrum of quantum states at the transition state influences the detailed dynamical observables of a chemical reaction.

In the traditional formulation of TST due to Eyring [2, 3], the transition state corresponds to an activated molecule with the reaction coordinate frozen at a value corresponding to the barrier maximum, i.e. $s = s_b$. The activated molecule is thus characterized by a spectrum of discrete quantum levels corresponding to the bound motion of the collision complex with s held fixed. Taken as a function of the reaction coordinate, the corresponding density of states is minimal at the transition state in variational TST [4, 5]. The density of states, and thus the rate constant, can be computed approximately from the potential energy surface (PES) using a vibrationally adiabatic model [6]. It is of interest to determine whether the quantum states can be taken literally and in principle observed, or if the discrete spectrum of states is merely a formal construction. Clearly, the level positions will be sensitive to the choice of reaction coordinate and the bound mode–mode coupling. However, such formal ambiguities do not preclude the existence of a discrete assignable set of transition state levels, albeit shifted from zero-order predictions. A more serious matter is the coupling to the continuum through the reaction coordinate itself. Thus, the instantaneous transition state energy levels are effectively broadened even in the absence of nonadiabatic coupling. A clear observation of the level structure is only likely to be possible for the lowest lying states where the level spacings are larger than the intrinsic widths.

The characterization of the energy level spectrum of the transition state can be made more precise if the motion along the reaction coordinate exhibits dynamical trapping. For example, if sufficiently deep wells exist on the adiabatic potential surfaces, resonance states will exist and can be assigned quantum numbers corresponding to the activated complex. Such Feshbach resonances were long predicted from theory [7, 8], but have only recently been unambiguously observed in the laboratory [9–11]. As the matter of observing Feshbach resonances has been reviewed recently [12–15], we omit here a detailed discussion of this subject. Instead, we focus on cases where the low-lying vibrationally adiabatic surfaces are pure barriers (or exhibit wells too shallow to support resonances) and hence where TST

should be most valid. For such reactions, the dynamical trapping is merely the slowing down of the translational motion near the barrier maximum. Friedman and Goebel [16], Friedman and Truhlar [17] and Seideman and Miller [18] have noted that the *S*-matrix for the one-dimensional barrier passage problem exhibits complex energy poles that are in some ways analogous to those of Feshbach resonances. Corresponding Seigert-state [19] wave functions may be determined analytically for sufficiently simple one-dimensional barriers or by using the numerical spectral quantization method for multidimensional reactions [20–22]. These assignable quantum (or quantized) bottleneck states (QBS) are weakly localized near the adiabatic barrier and exhibit exponential decay in the time domain with a lifetime consistent with the closest pole to the real energy axis. The most important conclusion from this work is that the intrinsic width of the transition state levels should be approximately $\Gamma \sim \hbar\omega$, where ω is the barrier frequency of the adiabatic barrier. (Note that while the width might appear to go to zero for a flat-topped barrier, anharmonicity and nonadiabatic coupling then dominate to maintain a broad feature.) While the barrier frequency is generally expected to be of the same magnitude as the bound frequencies for the most coupled modes, a propitious factor of $1/2\pi$ multiples line-widths compared to level spacings and suggests that in principle the first few levels may often be observable.

An important advance in the study of the quantum structure of the transition state was made recently by Truhlar and co-workers [23–27]. By analysing the cumulative reaction probability obtained using converged numerical scattering simulations, they found clear signatures of the QBS for a number of three-atom reactions. Near the energy for QBS, discernable step-like features appeared in the cumulative reaction probability that were consistent with quantized thresholds to reaction. It was noted that the QBS 'controlled' reactivity in the sense that knowledge of the positions and widths of these states allowed the microcanonical rate constant to be reconstructed. The astonishing conclusion of more recent work is that the QBS control of the reaction extends even to the level of state-to-state DCS.

We divide our discussion of the observation of QBS into two parts: (1) those systems studied as full collision problems and (2) those systems studied as half-collisions. While the work of Truhlar and colleagues has clearly established the importance of QBS to the theory of chemical reactions, identifying unique signatures of the QBS in observables accessible to experiment represents a significant challenge. For bimolecular (i.e. collisional) reactions, impact parameter averaging washes out the clear step-like structures predicted by Truhlar and co-workers for single values of the total angular momentum. Deeper analysis of the state-resolved DCS and integral cross-sections (ICS) is required to establish the nature of the influence of the QBS. In half-collision experiments, such as those designed to study the energy-selected unimolecular decay rate, the problem of impact parameter averaging is largely avoided. However, the step-like features predicted for the unimolecular rate assume statistical dynamics for the complex that may be in question for particular systems. In principle, the cleanest observation of a QBS would be provided by transition state spectroscopy, another problem invoking half-collision dynamics. Neumark [28] has established the utility of electron photodetachment spectroscopy of negative ion precursors for identifying reactive resonances in neutral reactions. Analogously, a QBS is expected to yield a broad peak in the kinetic energy spectrum of the detached electron at the energy of the dynamical barrier. As transition state

spectroscopy has been the subject of a number of recent reviews, we omit any detailed review of transition state spectroscopy in this work.

2. The theory of barrier passage

The traditional dynamical formulation of TST [29] is based on an analysis of the barrier passage problem. The rate of a reaction is thus computed from the flux through a dividing surface situated at the top of a dynamical barrier parameterized by a reaction coordinate. When the quantized nature of the motion orthogonal to the reaction coordinate is considered, the multidimensional dynamics is governed by a set of vibrationally adiabatic potential curves [30]. In natural collision coordinates, the coordinate 's' represents distance along the minimum-energy path, while the orthogonal vibrational modes are described by the normal mode coordinates '$\boldsymbol{u}$'. In the simplest form, the vibrationally adiabatic theory is constructed assuming that the quantum numbers $\boldsymbol{n}$ corresponding to coordinates u are conserved during the collision [30, 31]. Thus, vibrationally adiabatic potential curves are obtained of the form

$$V_{\mathrm{ad}}(s;\boldsymbol{n}) = V_0(s) + \varepsilon_{\boldsymbol{n}}(s) \tag{2.1}$$

where $V_0(s)$ is the potential along the reaction path and $\varepsilon_{\boldsymbol{n}}(s)$ are the quantized state energies of the orthogonal vibrational motion. The rotational states of the transition state complex are most often represented using a separable rigid rotor model with geometries computed along the reaction path. Thus, in this picture, the threshold energy for the reaction is represented by a discrete set of quantized bottleneck energies. These energies can be labelled by the vector of internal quantum numbers of the orthogonal vibrations at the barrier, $E_{\boldsymbol{n}}^{\mathrm{QBS}}$, or by a simple scalar ordering, E_i^{QBS}. The QBS energies are approximately equal to the barrier energies of $V_{\mathrm{ad}}(s;\boldsymbol{n})$ and correspond to the lowest allowed rotational level. A more precise value of $E_{\boldsymbol{n}}^{\mathrm{QBS}}$ is provided by the real part of the Seigert state energy (see below).

While the vibrationally adiabatic theory of reactions (and, equivalently, microcanonical variational TST) has proven to be very useful in the computation of reaction rate constants, it has been regarded as a highly approximate representation of the detailed reaction dynamics. Indeed, the separation of time scales between the s-motion (slow) and the $\boldsymbol{u}$-motion (fast) required for the rigorous validity of the model are seldom satisfied for real reactions. Therefore, it was surprising and important when Truhlar and co-workers [23, 25–27] observed clear signatures of the QBS in the results of exact quantum scattering calculations at energies near the adiabatic barrier maxima. Despite the significant approximations made, the adiabatic model seems to capture the essence the dynamics near the transition state. In particular, it confirms the near separability of the dynamics along the reaction coordinate near the barrier upon which TST is based.

In the remainder of this section, the theory for the dynamics of barrier passage leading to QBS is reviewed. In section 2.1, the simple case of one-dimension barriers is considered. While such models are clearly unrealistic, the essential pole structure of the S-matrix underlying the QBS emerges in a transparent way. In section 2.2, the generalization of the results to higher dimensional dynamical treatments is presented.

2.1. *The quantum dynamics of one-dimensional barriers*

The quantum transmission of a particle through a one-dimensional potential barrier is characterized by a threshold in the transmission coefficient, $T(E)$, located at an energy near the barrier height, V_0. The parabolic barrier provides the simplest one-dimensional problem,

$$V(s) = V_0 - \frac{1}{2}ks^2 \tag{2.2}$$

which can be easily solved analytically to obtain

$$T(E) = \frac{1}{1 + \exp(2\pi(V_0 - E)/\hbar\omega)} \tag{2.3}$$

where $\omega = \sqrt{k/\mu}$ with μ being the particle mass. When taken as a function of a complex energy, z, $T(z)$ exhibits poles at

$$z_n = V_0 - i\hbar\omega\left(n + \frac{1}{2}\right) \quad n = 0, 1, \ldots \tag{2.4}$$

As discussed by Seideman and Miller [18], Seigert-state wave functions corresponding to these poles may be obtained simply by replacing ω with $i\omega$ in the harmonic oscillator eigenstates. A more realistic, yet analytically solvable, barrier is provided by the Eckart potential

$$V(s) = \frac{A\xi}{1+\xi} + \frac{B\xi}{(1+\xi)^2} \quad \text{with} \quad \xi = \exp(s/a) \tag{2.5}$$

The barrier height, barrier frequency and exothermicity for this potential are given by

$$V_0 = \frac{(A+B)^2}{4B} \tag{2.6}$$

$$\omega = \sqrt{\frac{1}{a^2\mu}\frac{(B^2 - A^2)^2}{8B^3}} \tag{2.7}$$

$$\Delta V = -A \tag{2.8}$$

respectively. The transmission coefficient was derived formally by Eckart [32] to be

$$T(E) = \frac{\cosh[2\pi(\alpha - \beta)] + \cosh[2\pi\delta]}{\cosh[2\pi(\alpha + \beta)] + \cosh[2\pi\delta]} \tag{2.9}$$

with

$$\alpha = \frac{1}{2}\sqrt{\frac{E}{C}} \quad \beta = \frac{1}{2}\sqrt{\frac{E-A}{C}} \quad \delta = \frac{1}{2}\sqrt{\frac{B-C}{C}} \quad C = \frac{\hbar^2}{8\mu a^2} \tag{2.10}$$

In the case of a symmetrical barrier, i.e. $A = 0$, it is easily shown that the complex energy poles are located at

$$E_n = \frac{\hbar^2 k_n^2}{2\mu} \tag{2.11}$$

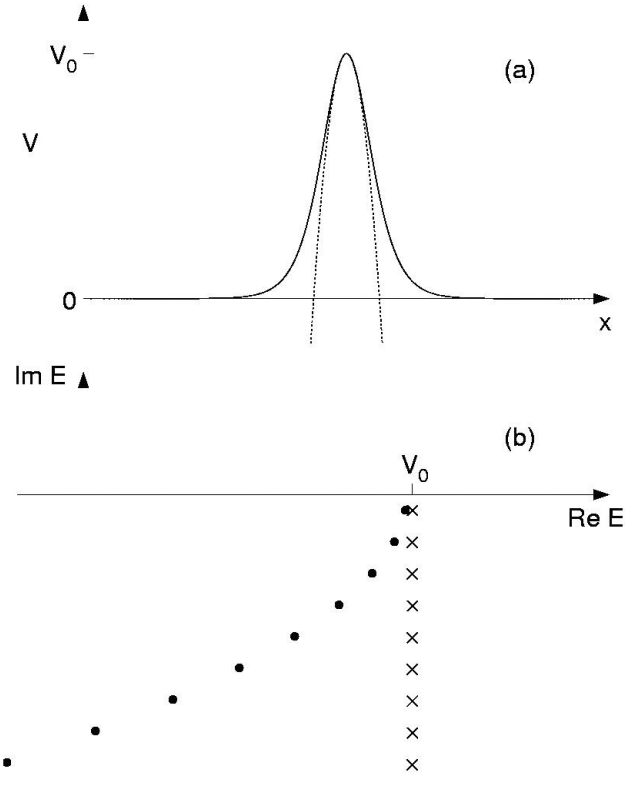

Figure 1. The Eckart barrier and the poles of the transmission coefficient in the complex E-plane. In the upper panel, we show the Eckart barrier with parameters chosen to mimic the $H + H_2$ reaction along with the parabolic approximation. The lower panel depicts the complex E-plane, where the poles from the Eckart potential are shown with dots while those for the parabolic barrier are shown with crosses.

where

$$k_n = \frac{1}{2a}\left[\sqrt{\frac{8\mu V_0}{\hbar^2 a^2} - 1} - i\left(n + \frac{1}{2}\right)\right] \tag{2.12}$$

As V_0 increases, holding ω constant, the Eckart poles approach those for the parabolic barrier. As illustrated in figure 1, the poles curve towards lower real energy as n increases. When $V_0 > \hbar\omega$, the position of the dominant pole (that pole closest to the real axis) is usually well approximated by the parabolic approximation as shown in the figure.

As the barrier-crossing problem exhibits a clear pole structure, it is tempting to invoke the model of scattering resonance to interpret the dynamics. Indeed, a number of traditional hallmarks of a resonance are fulfilled. For example, a time-dependent wavepacket launched from the vicinity of the barrier will 'hang-up' on the dominant pole and the long time dynamics is characterized by exponential decay of correlations and a stable form of the probability density. Furthermore, the collisional time-delay exhibits the classic peaking at the energy of the barrier maximum. Friedman and Truhlar [17] made the resonance connection more precise by a numerical study of the quantum dynamics of a series of one-dimensional

potentials. Starting with a double barrier potential exhibiting a clear shape resonance, the potential was deformed continuously into a single barrier. The pole for the shape resonance was mapped smoothly to the dominant pole for the barrier.

Despite the points of contact with resonance theory, the energy dependence of the barrier transmission probability exhibits a threshold and is clearly distinguishable from the traditional Lorentzian resonance profile of a Breit–Wigner isolated narrow resonance. Indeed, the barrier poles are never isolated. If the transmission coefficient is reconstructed as a pole expansion [15], the influence of the full analytic structure is apparent:

$$T(E) = 1 - \left| \prod_{n=0}^{\infty} \frac{k_n}{k - k_n} \right|^2 \tag{2.13}$$

Thus, if we attempt to decompose the S-matrix as a term from the dominant pole and a background contribution,

$$\mathbf{S}(E) = \mathbf{S}_{bg}(E) \left[\frac{E - z_0^*}{E - z_0} \right] \tag{2.14}$$

we find that the background term varies with energy about equally rapidly as does the pole term. Furthermore, we can construct a continuation process parallel to that of Friedman and Truhlar but starting from a potential exhibiting threshold behaviour.

In transition state spectroscopy, the occurrence of a potential (or dynamical) barrier yields a peak in a Franck–Condon spectrum centred at the corresponding energy of the barrier maximum. This phenomenon can be anticipated simply from the Condon reflection principle. A more detailed quantum mechanical analysis reveals that the line-shape for the barrier peak is distinct from the typical Fano-profile that applies to transitions to resonance states. Using a time-dependent formulation of the Franck–Condon spectrum, Sadeghi and Skodje [33] derived a line-shape formula containing three parameters: the barrier height V_0, the barrier frequency ω and a real asymmetry parameter ϕ that depends on the details of the overlap between the initial (ground state) wavepacket with the barrier potential

$$I(\Delta E) \propto e^{-2i\phi\eta} B(\eta, \eta^*) \quad \eta = -\frac{i\Delta E}{2\hbar\omega} + \frac{1}{4} \tag{2.15}$$

where B is the beta-function and $\Delta E = E - V_0$. Equation (2.15) can be viewed as a multiple-pole extension of the traditional single-pole Lorentzian profile. Unfortunately, the line-shape differences between Feshbach resonance and QBS are subtle and even modest amounts of rotational broadening or resolution error will mask the distinctions. Accurate theory is required to differentiate conventional resonance peaks from QBS peaks. Given an accurate PES, the spectral quantization method can be used to generate the wave functions associated with given peaks and thus make a precise assignment.

2.2. *Multidimensional bimolecular reactions*

To understand the influence of the QBS upon any real chemical reaction, we must consider the multidimensional character of the reaction. There are two essential generalizations required for the simple one-dimensional picture presented above. First, the possibility of internal excitation of the vibrational modes of the collision

complex must be included. Such excitations will generally lead to the influence of more than one QBS threshold on the reaction dynamics. Second, collisions occurring in three dimensions naturally involve a distribution of impact parameters. Hence, each QBS of the complex leads to a broad progression of rotational states, which may in turn cause the energy signatures of the QBS to be smeared over a range of energies.

We first consider a bimolecular reaction that takes place at a fixed value of the (conserved) total angular momentum, J. Then, the detailed reaction dynamics is described by a set of state-to-state reaction probabilities, $P_{\mathrm{R}}(\boldsymbol{n} \rightarrow \boldsymbol{n}'; E,J)$, where $\boldsymbol{n}$ ($\boldsymbol{n}'$) is the collection of initial (final) quantum numbers and E is the total energy. The reaction probabilities are sensitive to the barrier crossing dynamics and also to the rovibrationally nonadiabatic dynamics coupling in the entrance and exit channels. The cumulative reaction probability, $N_{\mathrm{R}}(E,J)$, is obtained by summing over all open channels of the reaction consistent with the conserved quantities (E,J),

$$N_{\mathrm{R}}(E,J) = \sum_{\mathbf{n},\,\boldsymbol{n}'}^{open} P_{\mathrm{R}}(\boldsymbol{n} \rightarrow \boldsymbol{n}'; E,J) \tag{2.16}$$

A less averaged quantity is the total reaction probability for the initial state $\boldsymbol{n}$, which is obtained by summing only over final product states

$$P_{\mathrm{R}}(\boldsymbol{n}; E,J) = \sum_{\boldsymbol{n}'}^{open} P_{\mathrm{R}}(\boldsymbol{n} \rightarrow \boldsymbol{n}'; E,J) \tag{2.17}$$

or an analogous final-state selected probability by summing, instead, over $\boldsymbol{n}$. The canonical rate constant, $k(T)$, is obtained by a Boltzmann average and an impact parameter sum of $N_{\mathrm{R}}(E,J)$ to obtain the well-known expression

$$k(T) = \frac{\int dE\, e^{-E/kT} \sum_{J} (2J+1) N_{\mathrm{R}}(E,J)}{hQ_{\mathrm{R}}(T)} \tag{2.18}$$

where $Q_{\mathrm{R}}(T)$ is the canonical partition function per unit volume of the reagents. Similar initial state specific rate constants are obtained by replacing $N_{\mathrm{R}}(E,J)$ with $P_{\mathrm{R}}(\boldsymbol{n};E,J)$ in equation (2.18).

The influence of the QBS is most transparent if we model $P_{\mathrm{R}}(\boldsymbol{n} \rightarrow \boldsymbol{n}'; E,J)$ and $N_{\mathrm{R}}(E,J)$ using the adiabatic theory of reactions. Thus, we assume that the internal quantum numbers of the collision complex are conserved through the course of the reaction and so an initial state, $\boldsymbol{n}_i$, correlates to a specific final state, $\boldsymbol{n}_i'$, we have

$$N_{\mathrm{R}}^{ad}(E,J) = \sum_{i}^{open} P_i^{ad}(\boldsymbol{n}_i \rightarrow \boldsymbol{n}_i'; E,J) \tag{2.19}$$

If the reaction probabilities for the individual adiabatic states are modelled using a set of parabolic barriers fit to the adiabatic potential curves, we have

$$N_{\mathrm{R}}^{ad}(E,J) = \sum_{i}^{open} \frac{1}{1 + \exp\left[2\pi\left(E_i^{\mathrm{QBS}}(J) - E\right)/\hbar\omega_i\right]} \tag{2.20}$$

where ω_i is the barrier frequency of the adiabatic barrier that will depend on J through the centrifugal modification to the adiabatic potential. Equation (2.20) is seen to exhibit a series of steps at the energies of the QBS that are resolved if the

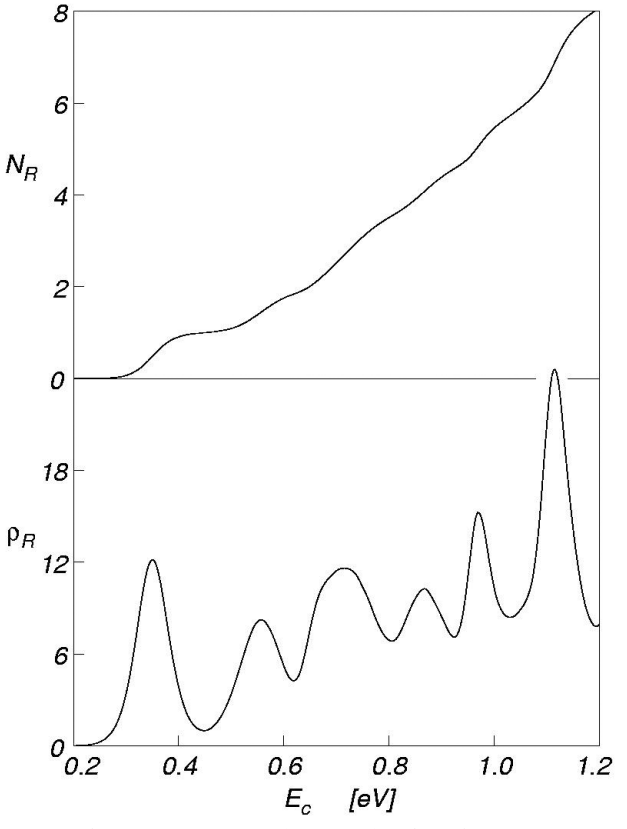

Figure 2. The converged quantum scattering results for the $D + H_2 \rightarrow HD + H$ reaction on the BKMP2-PES. The upper panel shows the cumulative reaction probability, $N_R(E,J=0)$ vs. E_C. The step-like features associated with the QBS threshold energies are clearly visible. In the lower panel, the density of reactive states, $\rho_R(E,J=0)$, vs. E_C exhibits easily identified peaks at the QBS energies.

QBS spacings are greater than $\hbar\omega_i/2\pi$. If the cumulative reaction probability is differentiated with respect to E, the resulting density of reactive states, $\rho_R(E,J) \equiv dN_R/dE$, shows peaks at the QBS energies that are more easily identified in practice.

Reactive steps in the cumulative reaction probability obtained from a quantum scattering calculation were apparently first noted by Bowman for the $O(^3P) + H_2$ reaction [34]. Truhlar and co-workers have analysed the exact quantum dynamics for a number of triatomic reactions using a treatment based on the QBS. They have found that the QBS were often quite apparent in $N_R(E,J)$ and even more strongly so in $\rho_R(E,J)$. As an illustration, we consider the $D + H_2 \rightarrow H + HD$ reaction that we have modelled using converged quantum scattering calculation for the BKMP2-PES. Chatfield *et al.* carried out a very similar study of this reaction on the LSTH-PES [27]. In the upper panel of figure 2, we show $N_R(E,J=0)$ vs. E_C, where we see that several of the reactive steps are clearly apparent. In the lower panel of figure 2 we plot $\rho_R(E,J)$ obtained by numerical differentiation of $N_R(E,J)$. The peaks in $\rho_R(E,J)$ are more apparent than the steps in $N_R(E,J)$. The peak positions were found to agree well with an independent determination of the QBS energies obtained using the spectral quantization method [35]. The QBS are labelled using the symmetric stretch and bending quantum numbers of a collinear triatomic

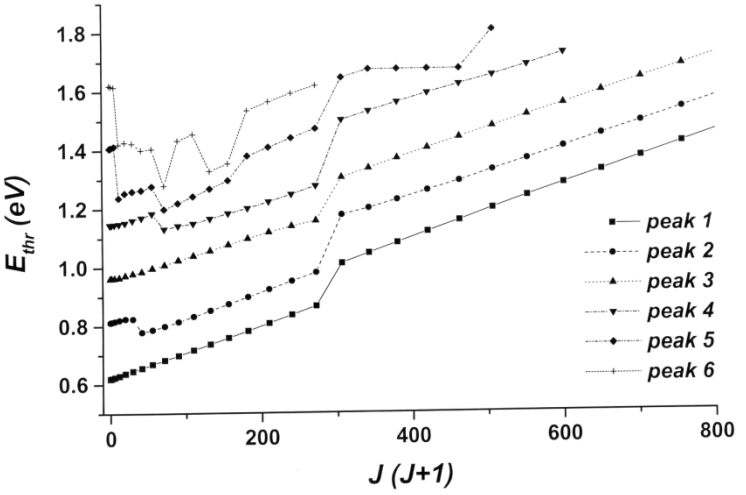

Figure 3. The peak positions of $\rho_R(E,J)$ vs. $J(J+1)$ for the $H+DH \rightarrow D+H_2$ reaction on the BKMP2-PES. The energies of the rotationally excited QBS are seen to be in reasonable agreement with the separable form, equation (2.21). Some of the peaks exhibit bifurcation vs. J, which accounts for the apparent discontinuities. Smooth progressions can be obtained using the fitting expression, equation (2.22).

molecule ($\nu_{ss}, \nu_b^{\Lambda}$). The exact QBS energies are found to be in reasonable agreement with the barrier heights for the corresponding vibrationally adiabatic potential curves. The reactive steps persist at higher values of angular momentum, although the density of states increases when $J > 0$ as the odd bending levels become symmetry allowed. The values of E_i^{QBS} as a function of total angular momentum can be obtained by finding the peak positions of $\rho_R(E,J)$. The resulting spectrum of energies is plotted in figure 3 (computed for the reverse reaction, H + HD) vs. the quantity $J(J+1)$. The levels are seen to exhibit J-shifting reasonably consistent with the separable expression for rotational levels of a linear molecule:

$$E_i^{QBS}(J) = E_i^{QBS}(0) + B_i J \cdot (J+1) \tag{2.21}$$

Finally, we note that several reactive steps are also clearly visible in the total reaction probability, $P_R(\boldsymbol{n}; E, J)$, shown in figure 4 for $J=0$ for the ground state of p-H_2.

As emphasized by Truhlar and co-workers, the QBS control the reactive flux by providing a set of discretely spaced thresholds to reaction. In principle, we can model the actual energy dependence of $N_R(E,J)$ based solely on the properties of the QBS. Because TST is approximate and thus the adiabatic barriers are recrossed, it is necessary to introduce transmission coefficients into equation (2.20) to obtain an accurate result

$$N_R(E,J) = \sum_i^{open} \frac{\kappa_i}{1 + \exp\left[2\pi\left(E - E_i^{QBS}(J)\right)/\hbar\omega_i\right]} \tag{2.22}$$

Using equation (2.22) with κ_i determined as numerical fitting parameters, it is possible to obtain a representation of $N_R(E,J)$ nearly indistinguishable from the exact result. The need to obtain κ_i from the exact scattering calculation is a limita-

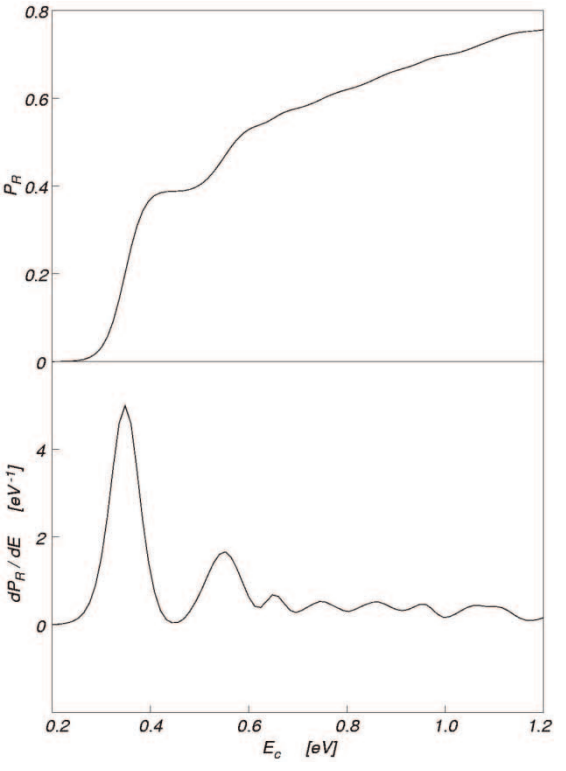

Figure 4. Upper panel: the total reaction probability $P_R(\boldsymbol{n};E,J=0)$ for $D+H_2(0,0)$ vs. E_C. Lower panel: the derivative of $P_R(\boldsymbol{n};E,J=0)$ with respect to energy exhibits peaks at the QBS energies.

tion on the predictive power of this method. However, a reasonable TST-level result is obtained by simply setting $\kappa_i = 1$.

For a bimolecular chemical reaction, neither $N_R(E,J)$ nor $P_R(\boldsymbol{n};E,J)$ is an accessible experimental observable. The influence of the QBS must, instead, be sought in the scattering cross-sections. Such observations necessarily involve an explicit averaging of the impact parameter of the collision and hence a sum over contributions from different values of J. The QBS energies, which act as threshold energies, progressively shift to higher energy with J, as in equation (2.21). Thus, a single threshold energy E_i^{QBS} for fixed J is replaced by a rotational progression of thresholds and we would expect the step-like feature to be smeared out in the energy dependence of the cross-sections. Indeed, numerical scattering calculations indicate that the reactive steps are masked by impact parameter averaging. Consider the energy dependence of the excitation function for the $D+H_2 \rightarrow HD+H$ reaction, which is the sum of the integral cross-sections for all final states of the reaction from a fixed initial state. This quantity is the full scattering analogue of the $P_R(\boldsymbol{n};E,J)$, which clearly exhibited reactive steps. As seen in figure 5, the excitation function is smooth with little structure except the overall reaction threshold. While the QBS led to easily identifiable steps in the function $N_R(E,J)$, the laboratory observation of these states in a bimolecular collision requires an understanding of the influence of the bottleneck states on the scattering observables.

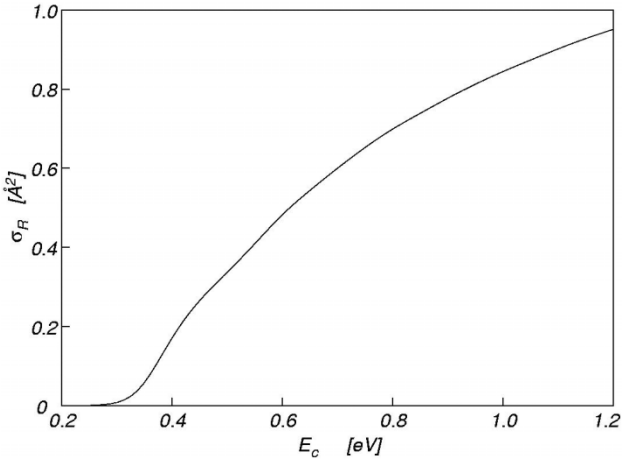

Figure 5. The excitation function vs. E_C for the reaction $D + H_2(0,0) \rightarrow HD + H$ computed using the BKMP2-PES. For the excitation function, the reactive steps are largely washed out by impact parameter averaging.

3. Strategies for observing quantum bottleneck states in reactive collisions

While the reactive steps associated with the QBS threshold energies are quite well resolved in the cumulative reaction probability or total reaction probability computed for fixed J, impact parameter averaging appears to wash out these structures in the excitation function of the reaction. Thus, the signature of QBS must be sought in the more highly resolved state-to-state DCS. This task, however, presents a significant theoretical challenge as it is not obvious a priori how the QBS will appear in such observables. However, recent progress has been made in unravelling this mystery. In this section, we review two different strategies for observing the QBS in collision experiments.

3.1. *Forward scattering peaks: manifestations of time-delay*

The measurement of a DCS holds the promise of at least partially undoing the impact parameter averaging of a collision. In classical potential scattering, the product observed at a selected COM angle, θ, corresponds to at most a few possible values of the impact parameter. While quantum effects and multidimensionality will partially obscure this relationship for real reactions, it is expected that the DCS is a useful tool for minimizing the blurring of averaging. It is conventional wisdom that backward scattering of the reaction products is dominated by low-impact parameter collisions while forward scattering results from high-impact parameter 'grazing' collisions. This viewpoint can be useful in analysing the differences of the reaction dynamics that proceed to various scattering angles. For example, the reaction barrier will be centrifugally shifted by a higher amount for forward scattering than for backward scattering.

Forward peaks of the final-state-selective DCS were identified by Lee and co-workers [36] as a potential signature for the existence of reactive resonances in the study of the $F + H_2$ reaction. While the precise mechanism for the formation of the forward peak was not fully elucidated, the physical picture was clearly that the resonance trapping permitted the F–H–H collision complex to rotate and form the forward peak. Essentially, the forward peak is a manifestation of time-delay.

If the complex lifetime were extremely long, then the DCS would show a forward–backward symmetry. A forward peak only suggests that the lifetime is less than a rotational period of the complex. Great care is required in concluding that forward peaks are the general fingerprints of resonance; however, direct dynamics can produce similar peaks (consider the hard sphere). In general, theory is required to firmly establish the connection between the observation and the mechanism. For the $F + HD \rightarrow HF + D$ reaction, Skodje and co-workers [10, 11] were able to conclude that the forward peaking in the DCS was in fact the result of a reactive resonance and the associated collisional time-delay [37].

The reaction dynamics occurring at energies near the maximum of an adiabatic barrier will exhibit a time-delay of the order of $\tau = 1/\omega$, where ω is the barrier frequency. This time-delay may give rise to forward scattering peaks of the reaction products that could provide an experimentally accessible signature of the QBS.

Recently, and independently, Harich *et al.* [35] and Althorpe *et al.* [38, 39] were able to conclude that forward peaks observed in the DCS for isotopic variants of the $H + H_2$ reaction were associated with collisional time-delay. Using a combined theoretical–experimental approach, Harich and colleagues [35, 40, 41] studied the $H + HD\,(v = 0, j = 0) \rightarrow D + H_2\,(v', j')$ reaction at a collision energy of $E_C = 1.2$ eV. The experiment was carried out using a molecular beam apparatus that used the Rydberg-atom time-of-flight detection scheme (Rydberg tagging) pioneered by Welge and co-workers [42]. Using an HI photolysis source for the hot H-atoms and a liquid nitrogen-cooled nozzle for the HD beam, the Rydberg tagging technique permitted the determination of DCS for each final rovibrational product state of the reaction. Figure 6 shows that the low-j' product states of the reaction exhibit very pronounced forward peaks in the DCS. The remaining reactive flux is localized mainly in the backward and sideways directions. The reaction was theoretically simulated using the quantum scattering method of Manolopoulos and co-workers [43] using the BKMP2-PES [44]. The result is shown in the lower panel of figure 6. A closer view of the comparison between theory and experiment for several product states is provided in figure 7. Theory and experiment were found to be in agreement to within experimental error bars. Furthermore, it was concluded that the forward scattered reaction product was rotationally colder and vibrationally hotter than other scattering angles.

While the forward peaking of the DCS could be simulated by theory, a more detailed analysis was required to determine the underlying mechanism. In particular, was the forward peaking associated with time-delay? The collisional time-delay as a function of scattering angle could be computed from the S-matrix using a method first proposed by Goldberger and Watson [45] and later studied by Kuppermann and Wu [46]. If the scattering amplitude is written as $f(\theta, E; \boldsymbol{n} \rightarrow \boldsymbol{n}')$, then the time-delay for scattering into angle θ for the reactive process $\boldsymbol{n} \rightarrow \boldsymbol{n}'$ is

$$\tau = \hbar \frac{d}{dE} Arg(f(\theta, E;\ \boldsymbol{n} \rightarrow \boldsymbol{n}')) \tag{3.1}$$

The time-delay function defined in this way generally exhibited irrelevant fine-scale structure associated, for example, with the minima of $|f|$ vs. angle [37]. Most of this structure can be eliminated by an average over final rotational and helicity states. In figure 8, we show the averaged time-delay at $E_C = 1.2\,\text{eV}$ vs. scattering

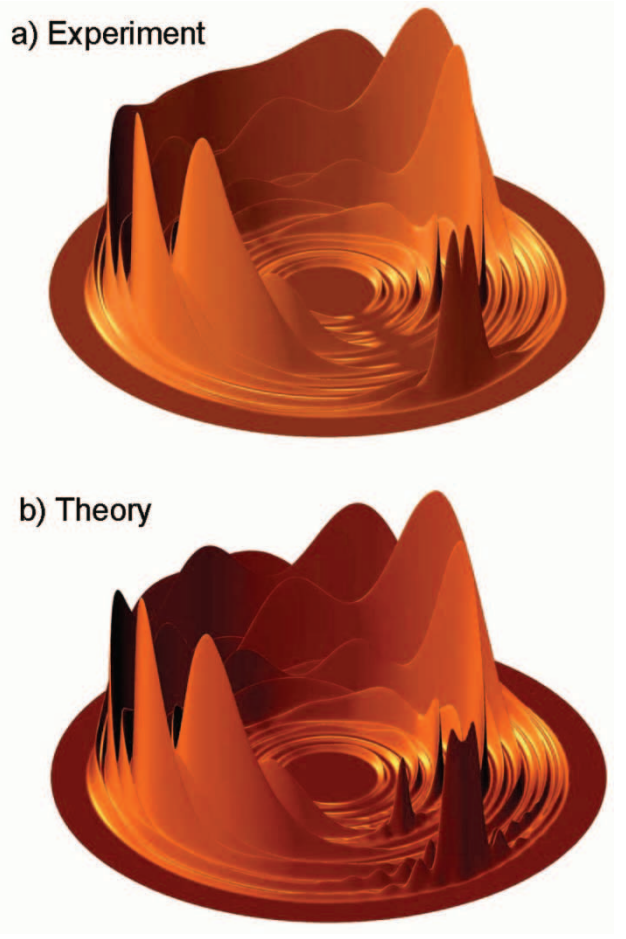

Figure 6. The differential cross-section for the reaction $H + DH(0,0) \rightarrow D + H_2(v', j')$ at $E_C = 1.2\,\text{eV}$. The angular coordinate represents the COM scattering angle and the radial coordinate the translational energy of the product. (a) Experimental result and (b) the result of a converged quantum scattering calculation on the BKMP2-PES.

angle. The time of collision clearly shows a peak in the forward direction that is of the order of 20 fs greater than, for example, backward scattering. This time-delay is significantly larger and more highly peaked than the normal kinematic forward enhancement observed in, for example, hard sphere scattering. Furthermore, the forward scattering naturally selects the reactive collisions occurring at the high-impact parameter, that is high J. If the DCS is computed using only partial waves up to a maximum $J_{\max}$, that is

$$\frac{d\sigma_R(J_{Max})}{d\Omega} = \frac{1}{4k_n^2}\left|\sum_{J=0}^{J_{Max}}(2J+1)\cdot d^J_{k,k'}(\pi-\theta)\cdot S_R(n\rightarrow n')\right|^2 \tag{3.2}$$

then contribution of various J-values may be inferred. In equation (3.2), (k, k') are initial and final helicity and d is the Wigner rotation function. As shown in

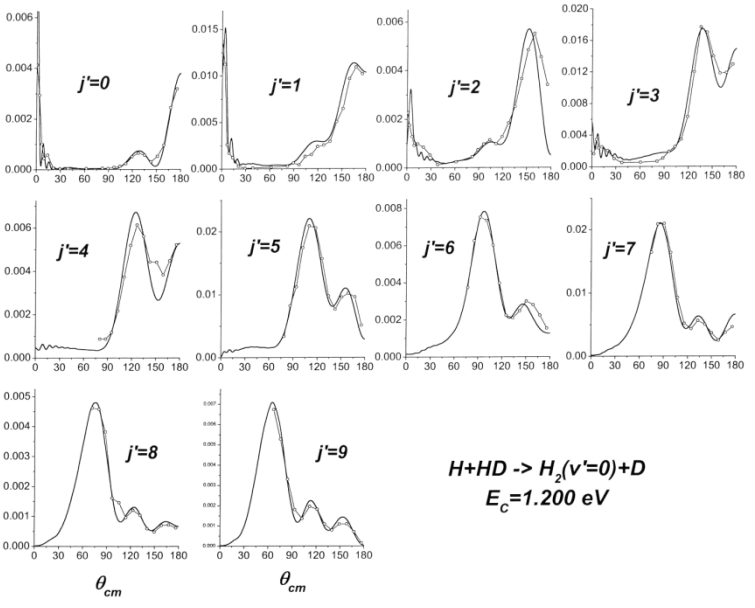

Figure 7. The differential cross-section for the reaction $H + DH(0,0) \rightarrow D + H_2(v',j')$ at $E_C = 1.2\,eV$ for individual product states in the $v' = 0$ manifold. The symbols are the experimental results and the solid lines are results of converged quantum scattering calculations.

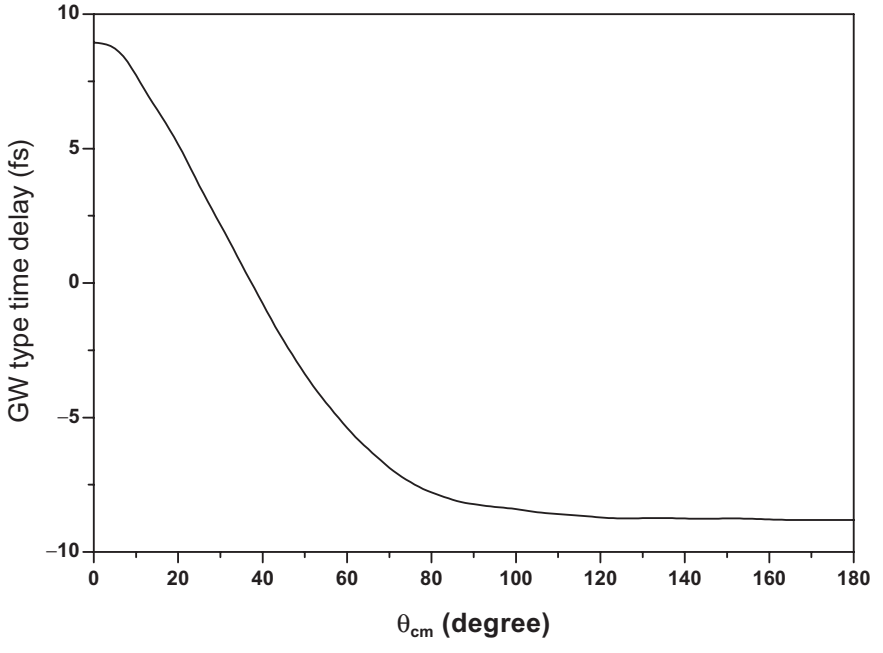

Figure 8. The angle-resolved time delay vs. θ for $H + HD(0,0) \rightarrow D + H_2$ at $E_C = 1.2\,eV$. The time delay, given by equation (3.1), has been averaged over final states to eliminate irrelevant fine-scale structure. The plot clearly reveals an additional 20 fs of time delay for scattering into the forward direction.

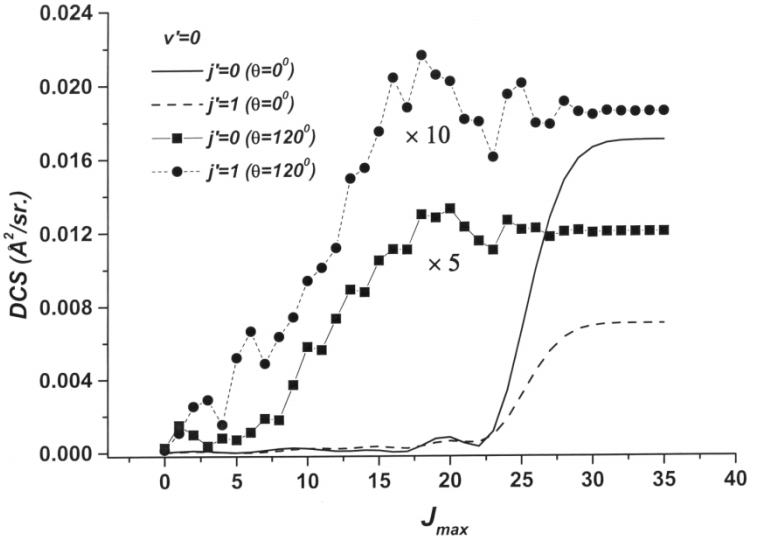

Figure 9. The reactive DCS at $E_C = 1.2$ eV for H + HD(0,0) computed as a partial sum (equation (3.2)) vs. J_{max}. The partial sum reactive DCS for the D + H_2(0,0) (and D + H_2(0,1)) product state in the forward direction is shown by the solid (dashed) curve. The same partial sum for the scattering angle of 120° is shown with symbols. The forward scattering is clearly the result of high-impact parameter collisions with $J \approx 25$.

figure 9, the forward peaking in the DCS for low-j' states at $E_C = 1.2$ eV is the result of high-impact parameter collisions rather narrowly localized around $J = 25$. At this value of the angular momentum, the vibrationally adiabatic barriers are centrifugally shifted upward by about 0.57 eV and the collision complex is 'rotating' at a rate of about 4° fs^{-1}.

To firmly establish the connection between the forward peak of the DCS and the QBS, it is necessary to examine the quantum reaction dynamics occurring at $J = 25$ near $E_C = 1.2$ eV. Does a QBS exist with these characteristics? The manifold of QBS was obtained using the spectral quantization method with the centrifugally shifted Hamiltonian corresponding to $J = 25$ and $\Omega = 0$. Thus, the energy spectrum of the transition state is given by

$$I(E) \propto \int_{-\infty}^{\infty} \langle \phi_{J=25}(0) \mid \phi_{J=25}(t) \rangle \cdot e^{iEt/\hbar} dt \tag{3.3}$$

where $\phi_{J=25}$ is a wavepacket evolving from a variationally optimized initial state near the transition state. As shown in figure 10, the lowest significant peak occurs precisely at $E_C = 1.2$ eV. The underlying state that gives rise to this peak is obtained by filtering the wavepacket at the peak energy

$$\Psi_E \propto \int_{-\infty}^{\infty} \phi_{J=25}(t) \cdot e^{iEt/\hbar} dt \tag{3.4}$$

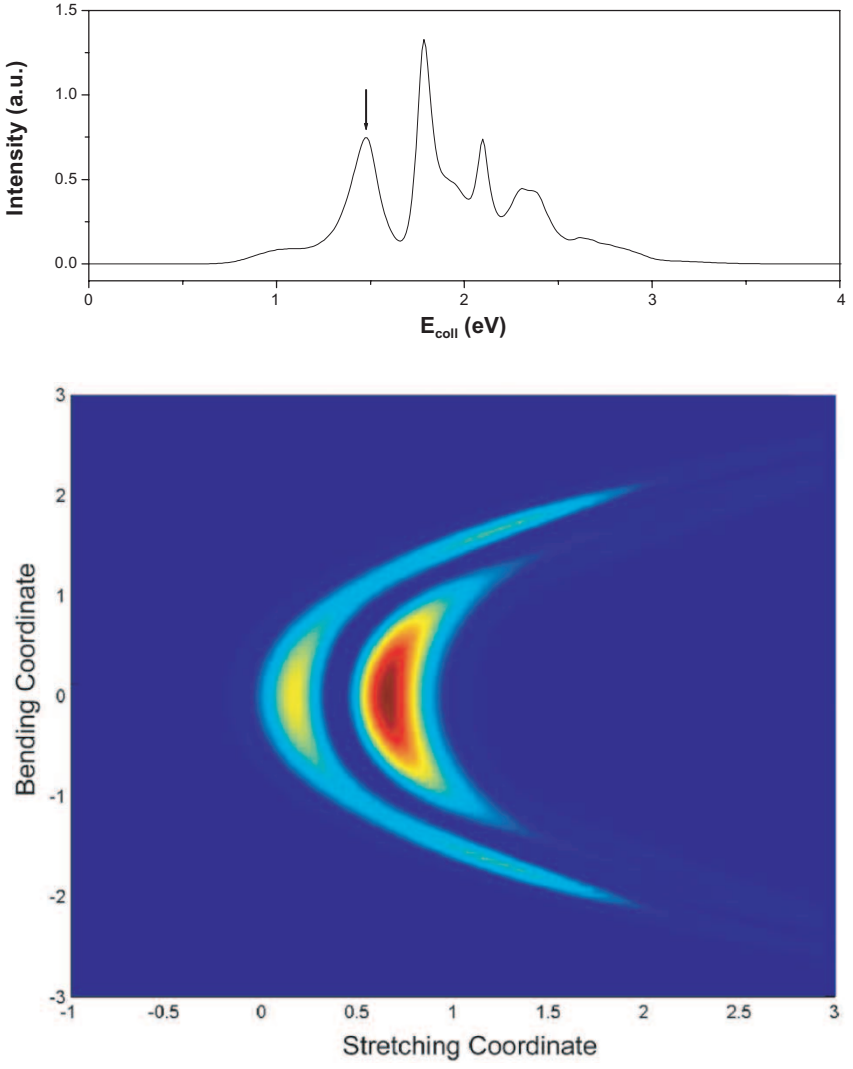

Figure 10. Characteristics of the QBS giving rise to the forward product scattering in H + HD. (a) The theoretical energy spectrum computed for the $J = 25$ centrifugally shifted Hamiltonian. The arrow indicates the peak associated with the QBS responsible for the forward scattering. (b) The probability density of the QBS obtained by spectral quantization plotted in normal mode coordinates. (c) The probability density of the QBS plotted in collinear Jacobi coordinates.

The resulting state at $E_C = 1.2$ eV is shown in figure 10 for the symmetric stretch and bending coordinates and also in collinear Jacobi coordinates. It is seen that the wave function is a mixed state involving $(v_{ss}, v_b^{\wedge}) = (1, 0^0)$ and $(0, 2^0)$. The mixing is a consequence of the near degeneracy of the two adiabatic barrier heights for $J = 25$.

The physical picture behind the formation of the forward peaks is now clear. As illustrated by the schematic in figure 11, the collision takes place at the high-impact parameter so that the (collinear) collision complex has already achieved an initial rotation angle of about 70° as the barrier is approached. The complex continues

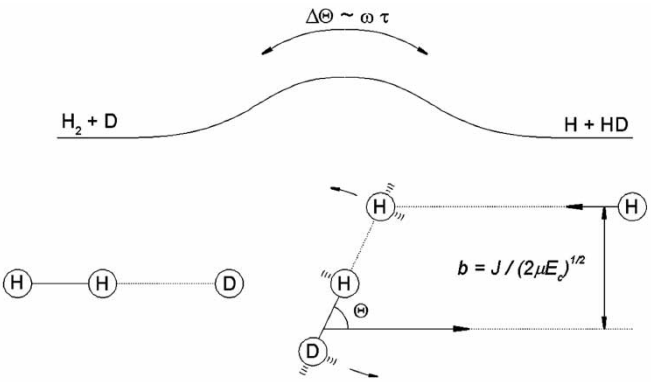

Figure 11. Schematic illustration of the time-delay mechanism for the formation of the forward peak. For collision energies very near the height of the centrifugally shifted adiabatic barrier (here, 1.2 eV), the collision slows down and the complex survives an extra $1/\omega \approx 20$ fs. During this added time, the complex continues to rotate at $4^\circ\,\mathrm{fs}^{-1}$, thus allowing the products to decay into the forward direction.

to rotate during the interval when the motion along the reaction coordinate has slowed down near the barrier maximum. The complex then decays in the forward direction leading to a peak at $\theta = 0^\circ$ when account is taken of the $1/\sin\theta$ geometric weighting factor.

Althorpe *et al.* [38, 39] and Zare and co-workers [47] have investigated the dynamics of the $H + D_2$ reaction using an approach that also combined theoretical and experimental efforts. The experiments were carried out using the PHOTOLOC (photo-initiated reaction analysed via the law of cosines) technique [48] with a $(2+1)$ REMPI time-of-flight detection scheme. The experiment permitted the determination of the DCS at a number of collision energies, although some angular averaging was implicit in the results because of the nature of the PHOTOLOC scheme. The theoretical dynamics was modelled using converged quantum scattering calculations, wavepacket simulations and quasi-classical trajectory calculations.

Although experimental convolutions over the PHOTOLOC instrument function appeared to wash out the forward scattering peaks for a number of product states, a clear forward enhancement was observed for the $D + HD\,(v' = 3, j' = 0)$ channel at $E_C = 1.64$ eV. An examination of classical trajectories contributing to this forward peak revealed some dynamical trapping near the transition state [49]. Allison *et al.* [50] noted that a centrifugally shifted vibrationally adiabatic barrier for $(v_{ss}, v_b) = (3,0^0)$ and $J = 33$ was quite close to the energy at which the peak was observed, thus implying a connection between the QBS and the forward peaks. A more dynamically exact treatment was provided by Althorpe *et al.* [38, 39] who carried out wavepacket calculations using an initial state that modelled an incoming plane wave. Plots of the wavepacket revealed that the backward scattering was prompt, while the forward scattering was delayed on the order of 25 fs as the probability density for the translational coordinate appeared to orbit the target. Such behaviour is consistent with trapping near a QBS although the precise assignment was not attempted. Aoiz *et al.* [49] have carried out quantum scattering calculations in combination with a complex angular momentum analysis that further elucidated the dynamics of the forward peak.

3.2. *Energy oscillations in state-to-state differential cross-sections*

While the forward scattering peaks can provide a signature of the time-delay associated with passage through a QBS, it is still desirable to obtain an energy-dependent manifestation of the QBS spectrum that would reveal a sequence of thresholds. Thus we consider whether some vestige of the staircase structure of reactive steps can survive impact parameter averaging in the scattering observables. The excitation functions for reactions that have been studied so far have failed to exhibit any clear sign of the QBS beyond the overall reaction threshold. However, in some cases, small undulations vs. E_C can be seen in the individual rovibrationally selected ICSs. Chao and Skodje [51], for example, noted such an effect in a quantum simulation for the process $H + D_2(v=0, j=0) \rightarrow HD(v'=0, j'=2) + D$, but the predicted structure was likely to be at or below the experimental detection limit. To minimize the blurring due to impact parameter averaging, it is again desirable to consider the state-to-state DCS vs. E_C at a fixed scattering angle. There are two broad issues that must be addressed before attempting this endeavour. First, while reaction steps are predicted in $N_R(E, J)$ at the QBS energies, how should the QBS thresholds manifest themselves in state-to-state reaction probabilities at fixed J? Second, how will the structures in the state-to-state S-matrix at various fixed J-values combine to yield the angle-dependent DCS?

A simple picture to interpret the energy dependence of the state-to-state reaction probabilities, based on the adiabatic model, has recently been advanced by Chao *et al.* [41] and Harich *et al.* [35]. As illustrated by the schematic diagram in figure 12, the adiabatic potential curves correlate the initial and final rovibrational states along the reaction coordinate. As no single rovibrational state will dominate the product distribution for any reaction with an appreciable barrier, it is essential to include the coupling between the different adiabatic curves. We note that adiabatic curves generally become more widely spaced near the barrier as the rotational levels correlate to bending states near the transition state. The strongest nonadiabatic coupling tends to occur away from the barrier in the entrance and exit valleys at, for example, avoided crossings [52]. In the language of TST, the dynamics along the reaction coordinate in the vicinity of the barrier is nearly separable. Thus, Harich *et al.* [35] conjectured that the reaction dynamics could be approximated using one-dimensional adiabatic dynamics near the barrier with the coupling introduced further out in the entrance and exit valleys. The **S**-matrix is then approximated by expression

$$\mathbf{S}(E) = \mathbf{S}_0^- \, \mathbf{S}_{na}^- \, \mathbf{S}_b \, \mathbf{S}_{na}^+ \mathbf{S}_0^+ \tag{3.5}$$

where $\mathbf{S}_0^{\pm}$ and $\mathbf{S}_{\mathrm{na}}^{\pm}$ represent the free asymptotic and the curve-hopping dynamics, respectively, in the entrance (exit) channels and $\mathbf{S}_b$ is the uncoupled propagation along a series of barriers near the transition state. Near a QBS energy (i.e. a barrier maximum), a new term in $\mathbf{S}_b$ will switch on. The effect of this threshold behaviour in the full $\mathbf{S}(E)$ is then to coherently redistributed among the channels through $\mathbf{S}_{na}^{\pm}$. The physical picture resulting from this model is that of a set of interfering pathways through the QBS, as illustrated in figure 12a. Hence, incident flux from a given initial state is redistributed over several adiabatic curves by $\mathbf{S}_{na}^+$, then passes the transition state on uncoupled curves $\mathbf{S}_b$ and is again coupled by $\mathbf{S}_{na}^-$ in the exit channel. For a very broad class of model problems, the $P_R(\boldsymbol{n} \rightarrow \boldsymbol{n}'; E, J)$ predicted by this scheme exhibits the behaviour illustrated in figure 12b. The QBS thresholds are seen to

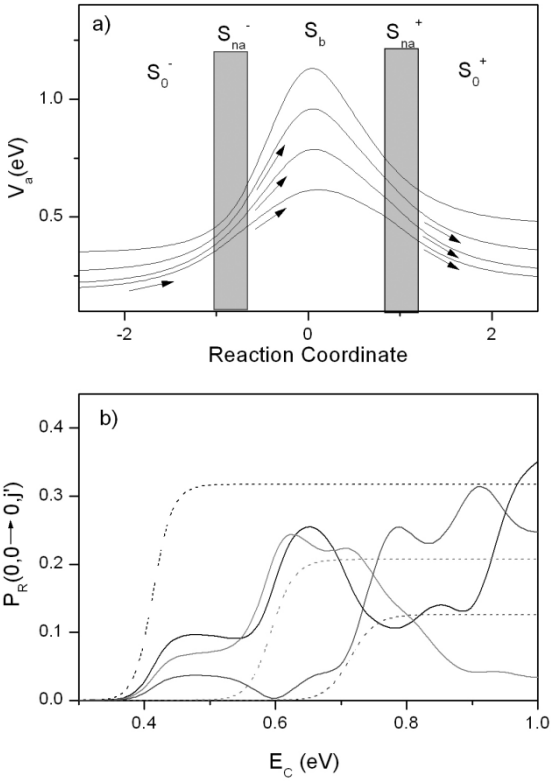

Figure 12. A schematic diagram illustrating the influence of QBS on the state-to-state reaction probabilities for a chemical reaction. (a) Several vibrationally adiabatic curves are sketched. The incident reagent flux is distributed over several adiabatic curves through the entrance channel nonadiabatic coupling term, S_{na}^{-}. The flux proceeds across the transition state on the uncoupled adiabatic curves via S_b. The flux is then redistributed again over the final product states by the exit channel nonadiabatic coupling term S_{na}^{+}. (b) The oscillating curves are state-to-state reaction probabilities obtained using a sequence of Eckart barriers and any physically reasonable form of the coupling matrix. The dashed curves are the reaction probabilities if the exit channel coupling is switched off.

induce a set of out-of-phase oscillations in the individual state-to-state probabilities. When the initial and final states are summed to obtain N_{R},

$$N_{\mathrm{R}} = \sum_{i,f} \left| \langle f | \mathbf{S}_0^- \cdot \mathbf{S}_{na}^- \cdot \mathbf{S}_b \cdot \mathbf{S}_{na}^+ \cdot \mathbf{S}_0^+ | i \rangle \right|^2 = \sum_i |\langle i | \mathbf{S}_b | i \rangle|^2 \tag{3.6}$$

the effect of the nonadiabatic couplings is averaged out leaving an expression analogous to equation (2.20) for the reactive steps. In fact, the peaks of the out-of-phase oscillations for the various $\boldsymbol{n} \rightarrow \boldsymbol{n}'$ transitions add together to form the reactive steps. The out-of-phase oscillations in $P_{\mathrm{R}}(\boldsymbol{n} \rightarrow \boldsymbol{n}'; E, J)$ have been observed in a number of reactions studied by using accurate quantum scattering calculations. For example, Chao *et al.* [41] have analysed the oscillation in $P_{\mathrm{R}}(\boldsymbol{n} \rightarrow \boldsymbol{n}'; E, J)$ vs. E for the H + HD reaction and established the close connection to the QBS energies. The staircase structure of $N_{\mathrm{R}}(E, J = 0)$ in H + HD and the underlying oscillations in the state-to-state reaction probabilities are represented in figure 13.

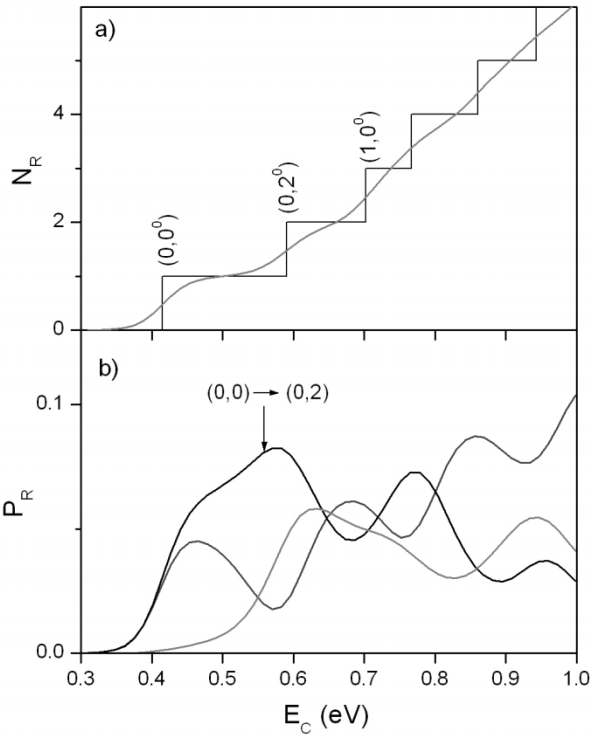

Figure 13. The reactive steps occurring in $N_R(E,J=0)$ for the H + HD reaction vs. energy. Also plotted are several individual state-to-state reaction probabilities. The plot is intended to illustrate how the out-of-phase oscillations of the reaction probabilities add to form the reactive steps.

The DCS is constructed from a coherent sum of contributions from different partial waves, for example in an atom + diatom reaction

$$\frac{d\sigma_R}{d\Omega} = \frac{1}{4k_n^2}\left|\sum_{J=0}^{\infty}(2J+1)\cdot d^J_{k,k'}(\pi-\theta)\cdot S^J_R(\boldsymbol{n}\rightarrow\boldsymbol{n}')\right|^2 \tag{3.7}$$

Thus, the influence of QBS that appear as oscillations in the individual S-matrix elements (as described above) are summed over to obtain the DCS. Thus, we might expect the structures to be washed out. As we have noted, however, the DCS tends to minimize the impact parameter averaging that obscures most structure in the ICS. Using various stationary phase approximations, Miller [53] showed that the DCS may be represented semiclassically by

$$\frac{d\sigma_R(\boldsymbol{n}\rightarrow\boldsymbol{n}')}{d\Omega} \approx \frac{d\sigma_{el}}{d\Omega}\cdot P_R(\boldsymbol{n}\rightarrow\boldsymbol{n}';E,J(\theta)) \tag{3.8}$$

where σ_{el} is a smooth elastic-like cross-section and $J(\theta)$ relates the scattering angle to J through the classical deflection function. Backward scattering is expected to correspond to $J=0$. Hence the oscillatory structure vs. E of $P_{\mathrm{R}}(\boldsymbol{n}\rightarrow\boldsymbol{n}';E,J=0)$ should be manifested in the DCS observed at $\theta=180^\circ$. Because for higher J, $P_{\mathrm{R}}(\boldsymbol{n}\rightarrow\boldsymbol{n}';E,J)$ vs. E generally exhibits a 'J-shifted' oscillatory behaviour, we would expect that the peaks of the backward oscillations will develop smoothly into

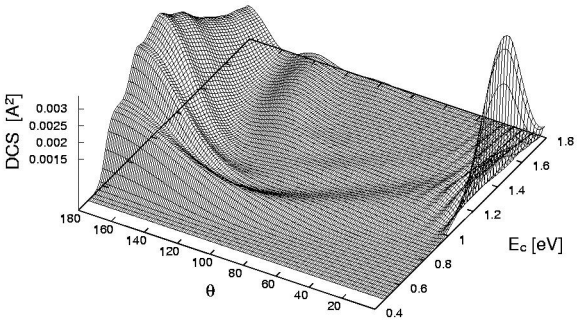

Figure 14. The DCS for the process $H + D_2(0,0) \rightarrow H + HD(0,0)$ vs. (E_{tot},θ) computed using quantum scattering theory. Ridge structures are seen to emanate from the peaks of the energy oscillations apparent in the backward scattering.

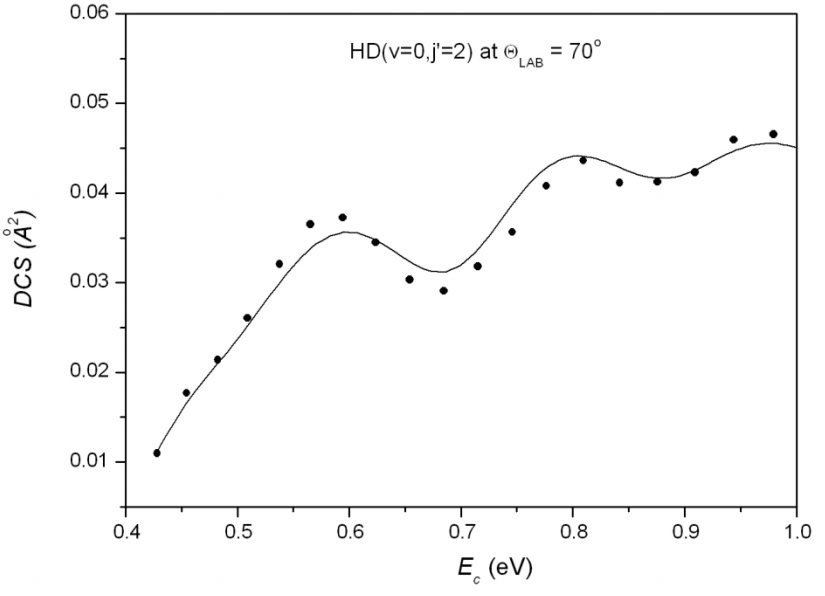

Figure 15. The DCS for the process $H + D_2(0,0) \rightarrow H + HD(0,2)$ vs. E_C. The laboratory scattering angle was held fixed at $\theta_L = 70^\circ$, corresponding to near backward scattering in the COM frame. The experimental results are shown with symbols while the predictions of quantum scattering theory are represented by a solid curve.

ridges in the E–θ plane. Miller and Zhang [54] have suggested searching for the ridge structures as a signature of 'elusive' reactive resonances. Indeed, Skodje *et al.* [11] have found that such a ridge exists for the resonance-mediated $F + HD \rightarrow HF + D$ reaction. For the $H + H_2$ family of reactions, the ridge structures are apparent in theoretically calculated DCSs [54, 55]. For example, in figure 14 we show a clear ridge for the process $H + D_2 \rightarrow HD + D$. In this example, as well for most other ridges observed in the $H + H_2$ family of reactions, the ridges tend to correspond to the QBS oscillations and not to traditional Feshbach resonances.

The energy dependence of the DCS for $H + D_2 \rightarrow HD + D$ was recently investigated by Dai *et al.* in an explicit attempt to observe the oscillations induced by the QBS thresholds. The experiment was similar to that conducted for the $H + HD$ reaction described above and used a beam of hot H-atoms crossed with a supersonic

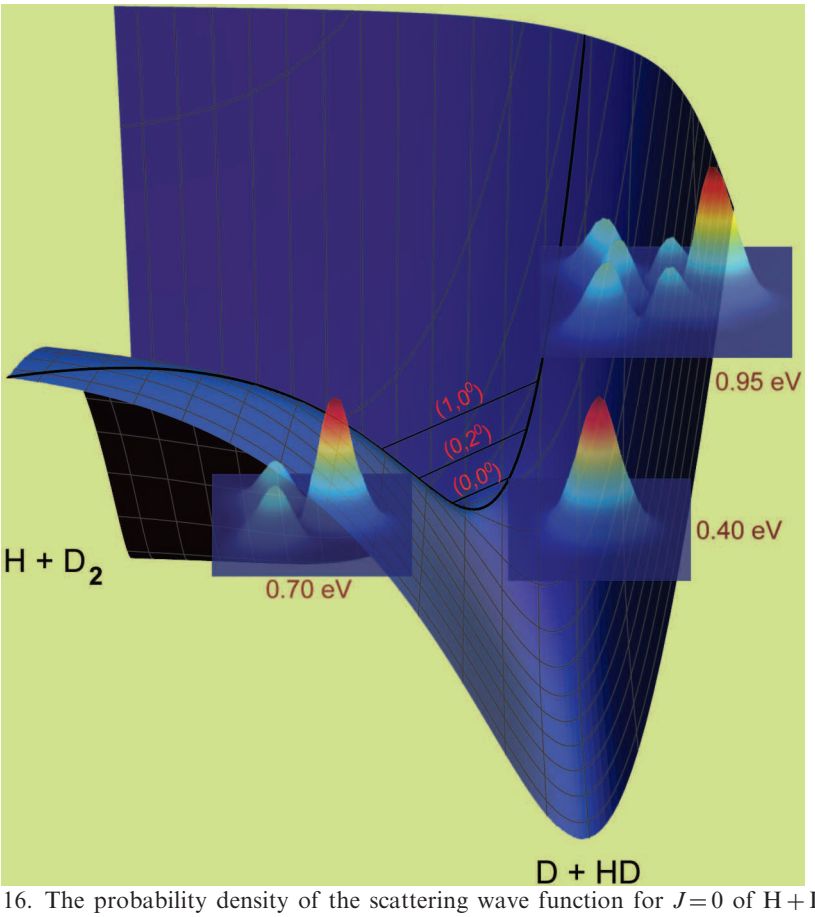

Figure 16. The probability density of the scattering wave function for $J=0$ of $H+D_2(0,0)$ sliced perpendicular to the reaction coordinate at the conventional transition state. The evolution of the probability density is illustrated at a series of collision energies.

D_2 molecular beam. The velocity of the D-atom product was again measured using the Rydberg-atom time-of-flight detection scheme. The collision energy was controlled through the use of a tunable dye laser for the HI-photolysis process. The oscillations in the state-to-state DCS predicted by quantum scattering theory were found to be most intense in the backward direction. Therefore, the detector was situated at a fixed laboratory angle $\theta_L = 70^\circ$ corresponding roughly to backward scattering and the collision energy was scanned over the range 0.42–1.0 eV. In figure 15, the DCS for the process $H + D_2(v=0, j=0) \rightarrow HD(v'=0, j'=2) + D$ is shown vs. E_C. The oscillations predicted by theory (shown as a solid line) are clearly apparent in the experimental result and the observations are in good quantitative agreement with theory. The oscillations were also observed for other product states and at other laboratory angles and are fully consistent with the picture outlined above.

Finally, it was possible to directly observe the influence of a sequence of QBS by examining the exact quantum dynamics near the transition state. Because for backward scattering the reaction is expected to be dominated by low-impact parameter collisions, the reaction dynamics for $J=0$ was considered. The station-

ary-state scattering wave function $\Psi_E(\boldsymbol{R})$ was obtained at a sequence of collision energies by (time) Fourier transform of a quantum wavepacket with the correct scattering boundary conditions for $H + D_2(0,0)$ and $J = 0$. The resulting states were sliced at the conventional transition state to obtain a probability density as a function of the symmetric stretch and bending coordinates. As seen in figure 16, the nodal pattern of the state evolves as the collision energy increases. At 0.4 eV, the wave function shows a single lobe at the saddlepoint and resembles the QBS with $(v_{ss}, v_b) = (0,0^0)$. At 0.7 eV, a pair of nodes in the bending coordinate indicates the influence of the $(0,2^0)$ state. At 0.95 eV, the $(1,0^0)$ as well as $(0,4^0)$ QBS is also shaping the probability density.

4. Observing quantum bottleneck states in unimolecular reactions

Similar to bimolecular reactions, unimolecular reactions also have barriers with QBS. Unimolecular reactions occur in a wide variety of problems where the activation process can take place through a number of distinct mechanisms. Through optical excitation, molecules can be promoted to electronically excited states. These excited molecules can then dissociate directly on the excited surface, or can undergo internal conversion to the ground-state surface followed by dissociation on this surface. If a molecule is thermally activated through a sequence of molecular collisions, it normally dissociates on its ground electronic surface. Infrared multi-photon dissociation can also induce a bond-breaking process on the ground-state surface by exciting molecules through vibrational-state ladders. Therefore, molecular fragmentation can occur in two broadly different ways: excited-state dissociation and ground-state dissociation. The topology of the dissociative-PES varies widely for different species, particularly for excited-state dissociation. If the PES on which a molecule dissociates is known, then, in principle, the dissociation rates and its dynamics through either semiclassical or accurate quantum dynamics calculations can be predicted. This is in fact the only way to obtain reliable information on molecular dissociation processes for dynamical systems that cannot be treated statistically. However, molecular dissociation on the ground state can usually be treated statistically. One of the most successful statistical theories calculating molecular dissociation rates is the RRKM theory, which was developed using the RRK model and extending it to consider explicitly vibrational and rotational energies and to include zero-point energies. Several minor modifications of the theory have been made since its conception, primarily as a result of improved treatments of external degrees of freedom.

The RRKM theory [56–61] is basically a microcanonical ensemble version of TST for calculating unimolecular reaction rates. RRKM theory is based on the additional assumptions that all vibrational states in the activated molecule are equally probable and that the vibrational energy flows freely among the different degrees of freedom at a rate much faster than the reaction rate. In RRKM theory, the rate constant $k(E)$ for unimolecular dissociation is given by

$$k(E, J) = N(E, J)/h\rho(E, J) \tag{4.1}$$

where $N(E, J)$ is the sum over the QBS for the active degrees of freedom in the transition state at E, $\rho(E, J)$ is the density of states for the active degrees of freedom in the reactant and h is the Planck constant. Earlier treatment of $N(E, J)$ is based on estimation of the vibrational frequencies of the vibrational modes orthogonal to

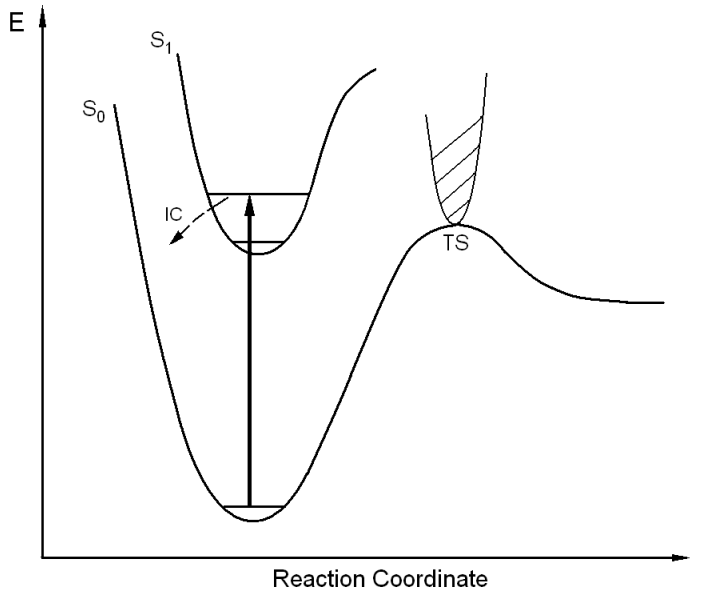

Figure 17. An ideal system for unimolecular dissociation studies to probe transition-state structures in the context of RRKM theory.

the reaction coordinate in the transition state. As *ab initio* calculations become more available, the vibrational frequencies of these vibrational modes in the transition state can be calculated. Near the unimolecular reaction threshold, where the QBS are sparse, the rate constant increases stepwise as the energy increases due to the sequential openings of different QBS pathways one by one. However, as the internal energy increases so does the number of vibrational states that can be accessed at the transition and therefore the steps will be more congested. This type of step structure has been seen in the cumulative reaction probability for elementary bimolecular chemical reactions. As shown in equation (3.1), this step structure lies intrinsically in the $N(E, J)$ function as more barrier states become accessible in a reaction.

The concept of QBS orthogonal to the reaction coordinate at the transition state is centrally important to unimolecular dissociation theory. Even though the notion of QBS has been used over many decades and is essential for the validity of the RRKM theory, the 'reality' of these states has been quite elusive for experimental verification. It can be suggested that the step structures predicted near the dissociation threshold in the unimolecular dissociation rate constants provide a reasonable opportunity to observe a progression of quantized states near the barrier. The issue is certainly to find a molecular system that is experimentally feasible for the measurement of energy-dependent dissociation rate constants near the unimolecular dissociation threshold. In addition, this system should be accurately described by RRKM theory. An ideal molecular system for such measurement should be more or less like the one depicted in figure 17, in which a molecule can be excited to its electronic excited state with monochromatic light, then undergo internal conversion to its ground electronic surface, on which the energy in the system is randomized before its dissociation. The system should also be rather simple

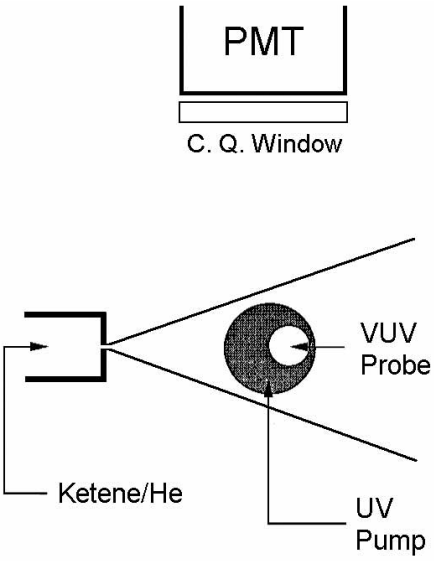

Figure 18. Experimental scheme for the VUV LIF detection of CO products from ketene photodissociation used by Moore *et al.* [62, 63].

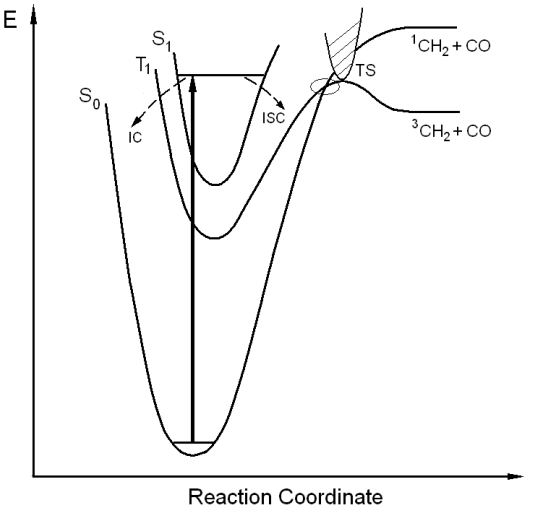

Figure 19. The three lowest potential-energy surfaces of ketene along the reaction coordinate. The ketene molecule is excited by a UV laser pulse to the first excited singlet state (S_1), undergoes internal conversion to S_0 and intersystem crossing to T_1 and dissociates into $^1CH_2(a\ ^1A_1) + CO$ (singlet channel) or $^3CH_2\ (X\ ^3B\ ) + CO$ triplet channel) fragments.

while statistical theory can still apply. Such an ideal system for measurement is nevertheless difficult to find and indeed has not yet been found.

In the early 1990s, the Moore group in Berkeley [62, 63] performed a groundbreaking experiment on ketene photodissociation in the UV region in an effort to detect QBS in the ketene dissociation through the triplet T_1 state. In this landmark experiment (see the experimental arrangement in figure 18), a cold ketene

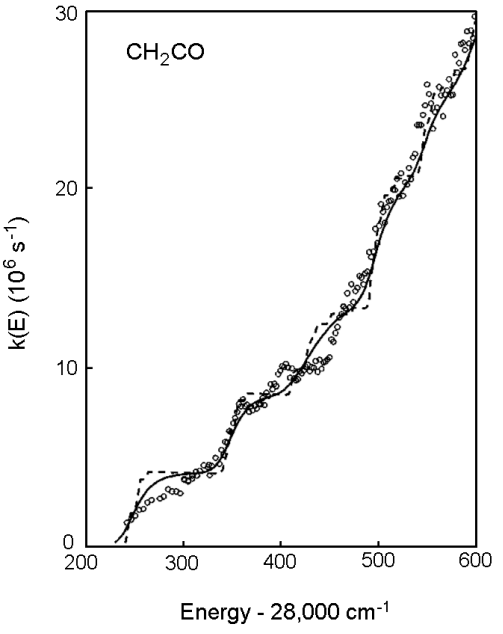

Figure 20. The measured rate constant for CH_2CO dissociation as a function of the photolysis energy. The solid line is an RRKM fit to the CH_2CO dissociation rate constants. The open circles are measured rate constants. The solid line is the RRKM fit without including the barrier tunnelling effect. The dotted line is the RRKM fit including the one-dimensional tunnelling with a barrier frequency of $40i$ cm^{-1}.

sample (4 K) prepared in a helium-seeded molecular beam was excited from the ground state S_0 surface to the electronically excited singlet surface, S_1, by a frequency doubled dye laser pumped by a Nd:YAG laser (figure 19). The CO-photodissociation product was subsequently detected using VUV laser-induced fluorescence (LIF) through the ($A\,^1\Pi \leftarrow X\,^1\Sigma_1$) transition. The pump–probe experiment allows the determination of the dissociation rate constants from the appearance rate of the CO product in a specific rovibrational state at different excitation energies. Figure 20 shows the energy dependence of the dissociation rate, $k(E)$. The circles are the experimental results while the solid line is the RRKM fit without considering the tunnelling effect near the barrier. The jumps observed in $k(E)$ were rationalized on the basis of the *ab initio* barrier transition-state vibrational levels. The step-like structure in the dissociation rate constant appeared to be explainable within the RRKM formalism in terms of barrier transition states orthogonal to the reaction coordinate, which become accessible in the transition state as the energy was increased. A full analysis of the observed energy profile of $k(E)$ was carried out by Kim *et al.* [63]. The first steps in $k(E)$ were assigned to the three lowest-energy modes in the transition state, the $H_2C{=}CO$ torsion, the $C{=}C{=}O$ bend and the CH_2 wag, treated in the first instance as a hindered rotor with an internal rotation barrier of 240 cm^{-1} and in the last two cases as small-amplitude normal vibrations with frequencies of 250 and 290 cm^{-1}, respectively. By comparison, the best theoretical values for the transition-state features were 384 cm^{-1} for the torsional barrier and 252 and 366 cm^{-1} for the corresponding harmonic vibrational frequencies. The threshold for triplet ketene fragmentation was pinpointed by the same analysis

of the $k(E)$ experiments, yielding a vibrationally adiabatic barrier of $1281 \pm 15\,\mathrm{cm}^{-1}$ for the exit channel, which is about 40% less than the best *ab initio* prediction. If the accuracy of the various pre-1990 *ab initio* quantities is assumed to be valid, the central interpretations of the breakthrough experiments on triplet ketene fragmentation is consistent with electronic structure theory. The experimental result was in good agreement with the long-standing RRKM premise that the rate of such a reaction is controlled by flux through the quantized transition states near the reaction barrier.

The ketene result was first published in the 12 June 1992 issue of *Science* as a cover story along with a perspective by Marcus appearing therein, entitled 'Skiing the Reaction Rate Slopes' [64]. This result was heralded in the perspective as a breakthrough test in which novel experimental evidence was advanced in support of one of chemistry's most fundamental theories, that is the RRKM microcanonical form of TST. The step structure observed in the experiment was also regarded as a clear experimental verification of the barrier transition states that has been hypothesized in many important chemical reaction theories. A similar phenomenon was also observed in the acetaldehyde UV photodissociation in a later study by Leu *et al.* [65], where step-like structures also seem to be present in the energy-dependent dissociation rate constant.

It is without question that the ketene photodissociation study itself [62, 63] is a breakthrough because such careful measurement and rigorous testing of the RRKM theory has never been carried out previously. However, there are serious questions remaining unanswered in this work. First, it seems to be difficult to explain several details of the step-like energy dependence of the reaction rate using the standard RRKM theory in the original work. Second, when one-dimensional tunnelling corrections were incorporated into the RRKM modelling of triplet ketene fragmentation through the transition state, the empirical barrier frequencies for the triplet transition state were found to be in the range of $(100 \pm 40)i\,\mathrm{cm}^{-1}$ and significantly lower than either the direct *ab initio* results or reasonable extrapolations by a factor of at least 3. Third, the RRKM fits of $k(E)$ near the triplet ketene threshold gave a density of reactant states equal to $1.11 g_t$ times the Whitten–Rabinovich estimate, where g_t is the number of spin sublevels in the T_1 manifold strongly coupled by intersystem crossing to $S_{0,}$ while both experiment [66] on the singlet dissociation channel of ketene and direct state counts [67] achieved by an extensive theoretical anharmonic vibrational analysis [68] of the S_0 surface have shown recently that g_t is also very close to 1 rather than 3. The similarity of g_t between the singlet and triplet channel implies that triplet channel dissociation somehow shows some singlet characteristics. Furthermore, experimental investigation on the ketene photodissociation [69] shows evidence that strong vibrational coupling in triplet ketene between internal rotation about the C–C bond and wagging motion is responsible for preferential *a*-axis rotational excitation of the product. This specific dynamical effect needs to be included for future quantum scattering studies on the step-like structure in the ketene photodissociation.

Because of the importance of this work and the questions raised around it, this system has attracted considerable attention in the theoretical dynamics community. The questions raised in the experimental study of the ketene photodissociation have been investigated extensively. It is becoming clear that two issues are crucial to the understanding of the ketene photodissociation in the context of the RRKM theory on the triplet surface.

(1) The first concerns the dynamics of the internal conversion (IC) between S_1 and S_0, and the intersystem crossings (ISCs) between S_1 and T_1, and S_0 and T_1, as creation of a statistical ensemble of ketene molecules on the T_1 surface through ISCs from S_1 and S_0 is the prerequisite for the valid application of the RRKM theory in the ketene dissociation. It is very important that the ICS rate is much faster than the dissociation rate so that the bottleneck of the dissociation from the S_0 surface lies at the triplet transition state.
(2) The second issue concerns the shape of the barrier on the triplet T_1 surface as the effect of the tunnelling near the barrier has a significant effect on the shape of the step-like structures of the dissociation rate.

In the complete report on the UV ketene photodissociation by Kim *et al.* [63], vibrational frequencies for the triplet transition state on the top of the barrier have been calculated to be $523i\ \mathrm{cm}^{-1}$. The magnitude of the barrier frequency reflects the barrier thickness, which is crucial to the tunnelling effect. Obviously, if the barrier frequency is higher, the dissociation barrier should be thinner and allow tunnelling to occur more easily. Therefore, the barrier frequency has a direct effect on the shape of the step-like structures observed in the energy-dependent dissociation rate constants. A barrier frequency of $(100 \pm 40)i\ \mathrm{cm}^{-1}$ was used by Kim *et al.* to fit the step-like structure in the energy-dependent dissociation rate constant. In 1996, Gezelter and Miller [70] performed a detailed analysis of the effect of the barrier frequency on the shape of the energy-dependent rate constant using the quantum reactive scattering method with a discrete variable representation. The dissociation rates arising from the reduced dimensionality computations accounting for one or two internal modes gave good overall agreement with experiment, but the step-like features in the ketene photodissociation were washed out by tunnelling through the relatively narrow barrier predicted by the improved *ab initio* theory. Model calculations confirmed that a barrier frequency below $100i\,\mathrm{cm}^{-1}$ is required to recover the observed steps in $k(E)$. Gezelter and Miller [70] suggested three possibilities for the disagreement between the theory and experiment on the step-like structures observed in the ketene photodissociation: (a) there is another transition state on the surface, further out towards the product T_1 channel; (b) surface-hopping dynamics are taking place between the T_1 and S_0 PES; or (c) the *ab initio* barrier frequency is simply too large.

More recently, Kaledin *et al.* [71] have investigated the dynamics of internal conversions using direct surface-hopping classical trajectories where the energy and gradient are computed on the fly by means of state-averaged complete active space self-consistent field with a double-ζ polarized basis set. Three low-lying electronic states, singlets S_0 and S_1 and triplet T_1, are found to be involved in the process of photodissociation of triplet state ketene. The major photodissociation pathway to the triplet products was found to be $S_1 \rightarrow S_0 \rightarrow T_1 \rightarrow CH_2(X\,^3B_1) + CO(X\,^{1+})$. The theoretical results clearly show that the S_0–T_1 nonadiabatic transition creates the T_1 species nonstatistically at restricted regions of phase space and a large fraction of the T_1 species thus created dissociates almost immediately, leaving no time for equilibration of internal degrees of freedom on the triplet surface. Whether a specific T_1 trajectory dissociates rapidly or not is determined by the amount of C–C stretch vibration at the S_0–T_1 branch point. This detailed study suggested strongly that the T_1 photodissociation process is highly nonstatistical, thus making equilibrium-based statistical theories, such as RRKM theory, inapplicable

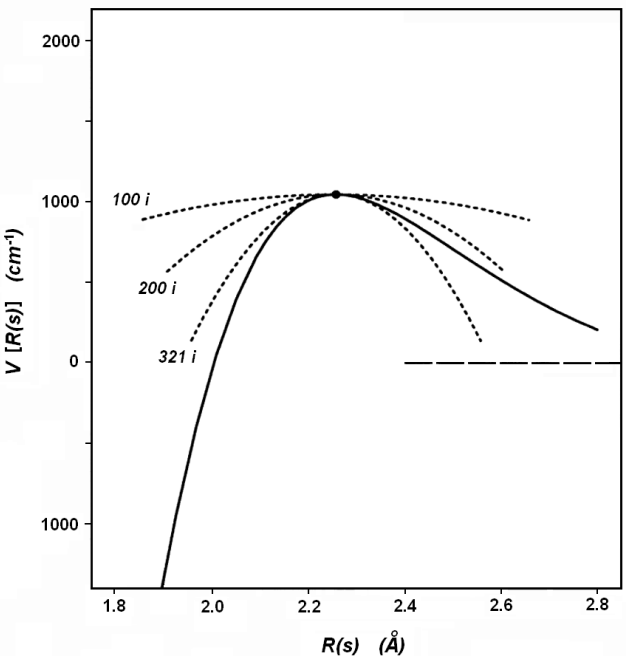

Figure 21. Expanded view of the potential-energy profile of the transition state for the triplet ketene in-plane transition-state fragmentation. The final theoretical curve (solid line) is shown in comparison to quadratic functions (dashed lines) with barrier frequencies of 100*i*, 200*i* and 321*i* cm^{-1}.

for computing the dissociation rate. The conclusion obtained by this study does not necessarily mean, however, that the step-like structure observed in the UV ketene photodissociation by the Berkeley group is not related to the barrier transition states. This structure could, in principle, still be related to the opening of different barrier transition states. As intersystem crossing dynamics between S_0 and T_1 can be energy dependent, the energy-dependent structure in the dissociation rate constant could thus be modulated by the ICS dynamics.

On the issue of the *ab initio* barrier frequency on the triplet surface, King *et al.* [72] have recently performed a very thorough theoretical investigation. They have rigorously mapped out the intrinsic reaction paths connecting the in-plane transition state to both the reactant and products at the TZ(2d1f, 2p) coupled-cluster singles and doubles (CCSD) level of theory. Final potential-energy functions along the entire reaction path have been determined with the aid of large atomic-orbital basis sets and extensive electron correlation treatments. The final theoretical curve is highly anharmonic in the transition-state region, displaying a classical barrier of 1045 cm^{-1}, a critical C–C distance of 2.257 Å and a barrier frequency of 321*i* cm^{-1}. Even though this high-level barrier frequency is significantly lower than the previously predicted *ab initio* barrier frequency of 523*i* cm^{-1} obtained by Kim *et al.* [63], it is still much higher than the *ca* 100*i* cm^{-1} barrier height required to retain the step-like structure in the triplet ketene dissociation rate constant. This detailed theoretical investigation strongly indicates that errors in the *ab initio* barrier frequencies are not responsible for the discord between quantum reactive scattering calculations and experiment concerning step-like structures in the dissociation

rate constant $k(E)$. This conclusion is supported by examination of the expanded view in figure 21 of the potential-energy profile of the transition state, in which the difference between a barrier with $100i$ cm^{-1} frequency and that with $321i$ cm^{-1} is so significant that it is unlikely to be caused by errors in the *ab initio* calculations.

Furthermore, there has been no clear experimental evidence that another transition state on the surface, further out towards the product T_1 channel, is present. Therefore, these theoretical studies show that the step-like structure observed in the ketene dissociation rate constant is probably not due to the barrier transition-state structures. However, the agreement between theory and experiment on the general trend in ketene triplet dissociation rate constants implies that the monotonic increase in the ketene dissociation rate constant is probably due to the sequential openings of the different barrier transition states even though the step-like structure is too broad to be observed. The observed step-like structure could be related to the energy-dependent intermolecular dynamics in view of the study of Kaledin *et al.* [71]. Considering the difficulties encountered in explaining all the details of the step-like structure observed in the original experiment using the standard RRKM theory, the above opinion seems to be not unreasonable.

From all the theoretical studies, it is also easy to conclude that the triplet ketene photodissociation seems not to be an ideal system for observing the structures of QBS in a photodissociation experiment due to its complex intramolecular dynamics and its barrier shape. It is also interesting to point out that a full quantum theoretical picture of how to observe QBS structure in a unimolecular reaction is yet clear. Much detailed investigation on both the theoretical and experimental fronts is needed to further understand the role of the barrier transition states in unimolecular dissociation processes.

In addition to ketene photodissociation, another similar study has been carried out on NO_2 photodissociation by the Wittig group [73–75] at USC using the femtosecond pump–probe technique. Time-resolved, subpicosecond resolution measurements of photoinitiated NO_2 unimolecular decomposition rates were measured for both molecular beam-cooled and room-temperature samples. The molecules were excited by 375–402 nm tunable subpicosecond pulses having bandwidths 220 cm^{-1} to levels that are known to be thorough admixtures of the $^2B_2$ electronically excited state and the $^2A_1$ ground electronic state. Subsequent decomposition was probed by a 226 nm subpicosecond pulse that excited laser-induced fluorescence (LIF) in the NO product. When increasing the amount of excitation over the dissociation threshold, an uneven, 'step-like' increase in the decomposition rate vs. energy was observed for the expansion-cooled samples (see figure 22). The step structures were spaced roughly by 100 cm^{-1}. These steps were tentatively assigned to the barrier bending vibration state structures at the transition state. In contrast to the expansion-cooled samples, the room-temperature samples exhibit a smooth variation in the reaction rate vs. photon energy. This is clearly an important experimental achievement in the study of unimolecular dissociation processes.

There are, however, several questions that need to be answered clearly in order to relate the step-like structures observed to barrier transition-state structures in the NO_2 photodissociation. First, even though the structure observed in the energy-dependent rate constant is very clear, its relation to the barrier bending vibration state remains be clarified because the 100 cm^{-1} bending is significantly lower than the bending frequency (758.6 cm^{-1}) of the NO_2 molecule. The transition

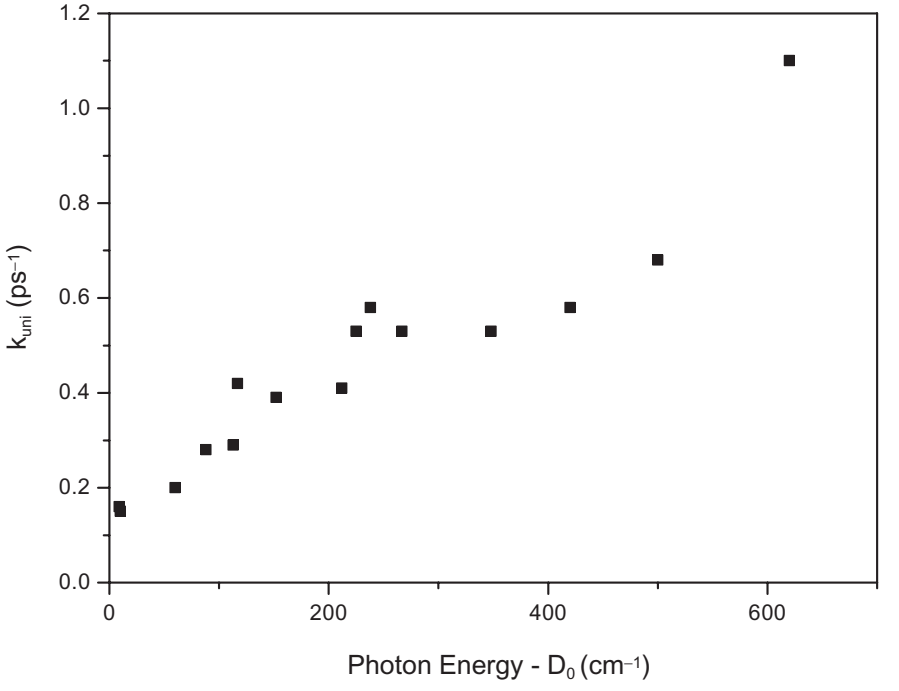

Figure 22. Unimolecular decay rate as a function of the quantity (photon energy $- D_0$) (i.e. essentially the energy in excess of reaction threshold) for expansion-cooled samples. The lengths of the rectangles represent the spectral bandwidths of the corresponding pump pulses.

state bending frequency at the transition state should be notably lower than the NO_2 bending frequency; whether it can be as low as $100\,cm^{-1}$ remains to be seen. Therefore, the assignment of the step-like structures is at most preliminary. Second, the assumption that rapid intramolecular vibrational redistribution (IVR) is much faster than dissociation could be in question because of very fast dissociation in NO_2 photodissociation. It is likely that the IVR rate is at most comparable to, if not slower than, dissociation. Therefore, this system could be dynamical instead of statistical. Therefore, the validity of applying the RRKM theory in this case could be called in question. As we have pointed out above, it is not completely clear in an exact theoretical picture how the energy-dependent dissociation rate structures are related to the transition-state structures in the dynamical dissociation process. In view of the above discussions, the possibility that the observed step-like structure in NO_2 photodissociation is due to some dynamical feature in the dissociation rather than to the transition-state structure cannot be ruled out entirely. This demonstrates once again the difficulties in trying to observe transition-state structures in a unimolecular dissociation process.

In another example of observing transition state structures in unimolecular processes, Choi *et al.* [76] have studied the *cis–trans* isomerization process. The *cis–trans* isomerization rates of *trans*,*trans*-1,3,5,7-octatetraene (OT) on the first excited singlet state potential surface were obtained as a function of vibrational energy by measuring the fluorescence lifetimes. An interesting stepwise increase in the isomerization rate with increasing energy was also observed. The authors attributed this stepwise structure to the quantization of the vibrational levels of

the transition state for the *cis–trans* isomerization of a double bond. The energy spacing of $80 \pm 10\,\mathrm{cm}^{-1}$ between the first two steps was tentatively assigned to an in-plane bending vibration of the transition state [77]. The isomerization threshold was determined to be $2140\,\mathrm{cm}^{-1}$ on the excited surface. This experimental observation of the step is clearly very interesting and also intriguing. The transition state of the *cis–trans* isomerization has not been mapped for this system, and a complete RRKM picture is lacking because of the limited information on the transition state. Therefore, the assignment of the step is based on the limited knowledge of the transition-state structures. A complete *ab initio* analysis on the transition state of *cis–trans* isomerization is needed to support the assignment of the step. It is also interesting to point out that statistical presumption of the RRKM theory is likely to be valid in this case because the IVR at even $2200\,\mathrm{cm}^{-1}$ for the OT molecule should already be significant, whereas the isomerization is relatively slow on a microsecond time scale.

Overall, significant advances in observing transition-state structures have been made for the above cases in unimolecular reaction processes. However, a clear-cut example has not yet appeared in the context of RRKM theory. More experimental and theoretical studies are required in order to search for an ideal and clear-cut example in this endeavour. Experimentally, it is necessary to look for an ideal system that allows us to observe the transition-state structures without the complication of intramolecular dynamics and the barrier effect as in the ketene photodissociation. Theoretically, it would be interesting to study photodissociation dynamics of an ideal molecular system at the full quantum dynamical level to see how the energy-dependent dissociation rate constant is related to the transition-state structures. This undertaking will certainly provide a clear map for observing QBS structures in unimolecular dissociation processes.

5. Conclusions

The concept of QBS has been essential in the interpretation of chemical reaction rates and reaction dynamics. However, observing these QBS has been a difficult task. In this article, we have provided an overview of the theory of the QBS and the current status of observing these states. In bimolecular reactions, collisional energy-dependent state-to-state differential cross-section measurement is the key to observing the QBS. Such measurement could significantly reduce the impact parameter averaging effect in crossed molecular beam studies. Recent studies of the $H + H_2$ reaction have demonstrated that observing QBS for this simplest chemical reaction is clearly possible experimentally with the idea described above. Even though observing QBS experimentally in the unimolecular dissociation of ketene has received great attention about a decade ago, the theoretical support is still not there for this case. It is clear that much of the detailed intramolecular dynamics in ketene remained to be clarified before this case can be regarded as a benchmark example of the observation of QBS in unimolecular reactions. This clearly demonstrates that even though the concept of QBS is extremely important, its observation remains elusive in unimolecular molecular reactions.

Acknowledgements

We are grateful to our collaborators, S. D. Chao, M. Gustafsson, S. A. Harich, D. X. Dai and C. C. Wang. We also thank D. G. Truhlar, C. B. Moore and

S. C. Althorpe for useful communications. This work was supported by the National Science Foundation of the USA, the Ministry of Science of China and the Chinese Academy of Sciences.

References

[1] Truhlar, D. G., Garret, B. C., and Klippenstein, S. J., 1996, *J. Phys. Chem.*, **100**, 12771.
[2] Eyring, H., 1935, *J. Chem. Phys.*, **3**, 107.
[3] Steinfeld, J. I., Francisco, J. S., and Hase, W. L., *Chemical Kinetics and Dynamics* (Prentice Hall, Englewood Cliffs, NJ, 1989).
[4] Keck, J. C., 1967, *Adv. Chem. Phys.*, **13**, 85.
[5] Truhlar, D. G., and Garret, B. C., 1984, *Annu. Rev. Phys. Chem.*, **35**, 159.
[6] Wigner, E. J., 1939, *Chem. Phys.*, **7**, 646.
[7] Levine, R. D., and Wu, S.-F., 1971, *Chem. Phys. Lett.* **11**, 557.
[8] Truhlar, D. G., and Kuppermann, A. J., 1972, *Chem. Phys.*, **56**, 2232.
[9] Weaver, A., Metz, R. B., Bradforth, S. E., and Neumark, D. M., 1988, *J. Phys. Chem.*, **92**, 5558.
[10] Skodje, R. T., Skouteris, D., Manolopoulos, D. E., Lee, S.-H., Dong, F., and Liu, K., 2000, *J. Chem. Phys.*, **112**, 4536.
[11] Skodje, R. T., Skouteris, D., Manolopoulos, D. E., Lee, S.-H., Dong, F., and Liu, K., 2000, *Phys. Rev. Lett.*, **85**, 1206.
[12] Liu, K., 2001, *Annu. Rev. Phys. Chem.*, **52**, 139.
[13] Chao, S. D., and Skodje, R. T., 2002, *Theor. Chem. Acc.*, **108**, 273.
[14] Fernandez-Alonso, F., and Zare, R. N., 2002, *Annu. Rev. Phys. Chem.*, **53**, 67.
[15] Chao, S. D., and Skodje, R. T., in *Modern Trends in Chemical Reaction Dynamics*. Part 2, edited by X. Yang and K. Liu (World Scientific, 2004).
[16] Friedman, W. A., and Goebel, C. J., 1977, *Ann. Phys.*, NY, **104**, 145.
[17] Friedman, R. S., and Truhlar, D. G., 1991, *Chem. Phys. Lett.*, **183**, 539.
[18] Seideman, T., and Miller, W. H., 1991, *J. Chem. Phys.*, **95**, 1768.
[19] Seigert, A., 1939, *J. Phys. Rev.*, **56**, 750.
[20] Sadeghi, R., and Skodje, R. T., 1993, *J. Chem. Phys.*, **98**, 9208.
[21] Sadeghi, R., and Skodje, R. T., 1995, *J. Chem. Phys.*, **102**, 193.
[22] Skodje, R. T., Sadeghi, R., Koppel, H., and Krause, J. L., 1994, *J. Chem. Phys.*, **101**, 1725.
[23] Chatfield, D. C., Friedman, R. S., Truhlar, D. G., Garret, B. C., and Schwenke, D. C., 1991, *J. Am. Chem. Soc.*, **113**, 486.
[24] Chatfield, D. C., Friedman, R. S., Truhlar, D. G., Garret, B. C., and Schwenke, D. C., 1991, Faraday Discuss. *Chem. Soc.*, **91**, 289.
[25] Chatfield, D. C., Friedman, R. S., Schwenke, D. C., and Truhlar, D. G., 1992, *J. Phys. Chem.*, **96**, 2414.
[26] Chatfield, D. C., Friedman, R. S., Lynch, R. S., Truhlar, D. G., and Schwenke, D. C., 1993, *J. Chem. Phys.* **98**, 342.
[27] Chatfield, D. C., Mielke, S. L., Allison, T. C., and Truhlar, D. G., 2000, *J. Chem. Phys.*, **112**, 8387.
[28] Neumark, D. M., 1992, *Annu. Rev. Phys. Chem.*, **43**, 153.
[29] Wigner, E. J., 1937, *Chem. Phys.*, **5**, 720.
[30] Miller, W. H., Handy, N. C., and Adams, J. E., 1980, *J. Chem. Phys.*, **72**, 99.
[31] Isaacson, A. D., and Truhlar, D. G., 1982, *J. Chem. Phys.*, **76**, 1380.
[32] Eckart, C., 1930, *Phys. Rev.*, **35**, 1303.
[33] Sadeghi, R., and Skodje, R. T., 1995, *Phys. Rev.*, A **52**, 1996.
[34] Bowman, J. M., 1987, *Chem. Phys. Lett.*, **141**, 545.
[35] Harich, S. A., Dai, D. X., Wang, C. C., Yang, X., Chao, S. D., and Skodje, R. T., 2002, *Nature*, **419**, 281.
[36] Neumark, D. M., Wodtke, A. M., Robinson, G. N., Hayden, C. C., Shobatake, R., and Lee, Y. T., 1985, *J. Chem. Phys.*, **82**, 3045.
[37] Chao, S. D., and Skodje, R. T., 2003, *J. Chem. Phys.*, **119**, 1462.
[38] Althorpe, S. C., Fernandez-Alonso, F., Bean, B. D., Ayers, J. D., Pomerantz, A. E., Zare, R. N., and Wrede, E., 2002, *Nature*, **416**, 67.

[39] Althorpe, S. C., 2002, *J. Chem. Phys.*, **117**, 4623.
[40] Harich, S. A., Dai, D., Yang, X., Chao, S. D., and Skodje, R. T., 2002, *J. Chem. Phys.*, **116**, 4769.
[41] Chao, S. D., Harich, S. A., Dai, D. X., Wang, C. C., Yang, X., and Skodje, R. T., 2002, *J. Chem. Phys.*, **117**, 8341.
[42] Schnieder., L., Seekamp-Rahn, K., Wrede, E., and Welge, K. H., 1997, *J. Chem. Phys.*, **107**, 6175.
[43] Skouteris., D., Castillo, J. F., and Manolopoulos, D. E., 2000, *Comput. Phys. Commun.*, **133**, 128.
[44] Boothroyd, A. I., Keogh, W. J., Martin, P. G., and Peterson, M. R., 1996, *J. Chem. Phys.*, **104**, 7139.
[45] Golderberger, M. L., and Watson, K. M., *Collision Theory* (Wiley, New York, 1964).
[46] Kuppermann, A., and Wu, Y.-S. M., 1995, *Chem. Phys. Lett.*, **241**, 229.
[47] Fernandes-Alonso, F., Bean, B. D., Ayers, J. D., Pomerantz, A. E., Zare, R. N., Banares, L., and Aoiz, F. J., 2001, *Angew. Chem., Int. Ed. Engl.*, **39**, 2748.
[48] Fernandes-Alonso, F., Bean, B. D., and Zare, R. N., 1999, *J. Chem. Phys.*, **111**, 1022.
[49] Aoiz, F. J., Banares, L., Castillo, J. F., and Sokolovski, D., 2002, *J. Chem. Phys.*, **117**, 2546.
[50] Allison, T. C., Friedman, R. S., Kaufman, D. J., and Truhlar, D. G., 2000, *Chem. Phys. Lett.*, **327**, 439.
[51] Chao, S. D., and Skodje, R. T., 2001, *Chem. Phys. Lett.*, **336**, 364.
[52] Nobusada, K., Tolsikhin, O. I., and Nakamura, H., 1998, *J. Chem. Phys.*, **108**, 8922.
[53] Miller, W. H., 1970, *J. Chem. Phys.*, **53**, 1949.
[54] Miller, W. H., and J. Z., Zhang., H., 1991, *J. Phys. Chem.*, **95**, 12.
[55] Aoiz, F. J., Herrero, V. J., and Saiz Rabanos,V., 1992, *J. Chem. Phys.*, **97**, 7423.
[56] Marcus, R. A., and Rice, O. K., 1951, *J. Phys. Colloid. Chem.*, **55**, 894.
[57] Marcus, R. A., 1952, *J. Chem. Phys.* **20**, 359.
[58] Marcus, R. A., 1990, *Philos. Trans. R. Soc. London, Ser.*, A **332**, 283.
[59] Robinson, P. J., and Holbrook, K. A., *Unimolecular Reactions* (Wiley, New York, 1972).
[60] Forst, W., *Theory of Unimolecular Reactions* (Academic Press, New York, 1973).
[61] Gilbert, R. G., and Smith, S. C., *Theory of Unimolecular and Recombination Reactions* (Blackwell, Oxford, 1990).
[62] Lovejoy, E. R., Kim, S. K., and Moore, C. B., 1992, *Science* **256**, 1542.
[63] Kim, S. K., Lovejoy, E. R., and Moore, C. B., 1995, *J. Chem. Phys.* **102**, 3202.
[64] Marcus, R., 1992, *Science*, **256**, 1522.
[65] Leu, G. H., Huang, C. L., Lee, S. H., Lee, Y. C., and Chen, I. C., 1998, *J. Chem. Phys.*, **109**, 9340.
[66] Wade, E. A., Mellinger, A., Hall, M. A., and Moore, C. B., 1997, *J. Phys. Chem.* A, **101**, 6568.
[67] Klippenstein, S. J., East, A. L. L., and Allen, W. D., 1996, *J. Chem. Phys.*, **105**, 118.
[68] East, A. L. L., Allen, W. D., and Klippenstein, S. J., 1995, *J. Chem. Phys.*, **102**, 8506.
[69] Morgen, C. G., Drabbles, M., and Wodtke, A. M., 1996, *J. Chem. Phys.*, **105**, 4550.
[70] Geselter, J. D., and Miller, W. H., 1996, *J. Chem. Phys.*, **104**, 3546.
[71] Kaledin, A. L., Seong, J., and Morokuma, K., 2001, J. *Phys. Chem.*, A **105**, 2731.
[72] King, R. A., Allen, W. D., Ma, B., and Schafer, H. F., 1998, III, Faraday Discuss. **110**, 23.
[73] Ionov, S. I., Davis, H. F., Mikhaylichenko, K., Valachovic, L., Beaudet, R. A., and Wittig, C., 1994, *J. Chem. Phys.*, **101**, 4809.
[74] Ionov, S. I., Brucker, G. A., Jaques, C., Chen, Y., and Wittig, C., 1993, *J. Chem. Phys.*, **99**, 3420.
[75] Wittig, C., and Ionov, S. I., 1994, *J. Chem. Phys.*, **100**, 4714.
[76] Choi, Y. S., Kim, T. S., Petek, H., Yoshihara, K., and Christensen, R. L., 1994, *J. Chem. Phys.*, **100**, 9269.
[77] Petek, H., Bell, A. J., Choi, Y. S., Yoshihara, K., Ounge, B., and Christensen, R. L., 1993, *J. Chem. Phys.*, **98**, 3777.